JACC: BASIC TO TRANSLATIONAL SCIENCE VOL. 9, NO. 5, 2024

ORIGINAL RESEARCH - PRECLINICAL

Thrombospondin-1 Drives Cardiac Remodeling in Chronic Kidney Disease

Sohel M. Julovi, MBBS, PhD,[a,b] Katie Trinh, BSc(Adv), MBBS,[a] Harry Robertson, BMedSc(Hons-I),[a,b,c] Cuicui Xu, BSc, PhD,[a] Nikita Minhas, PhD,[a] Seethalakshmi Viswanathan, MBBS,[b,d] Ellis Patrick, BSc(Hons), PhD,[a,c,e,f] John D. Horowitz, MBBS, PhD,[g,h,i] Daniel N. Meijles, PhD,[g] Natasha M. Rogers, MBBS(Hons), PhD[a,b,j]

VISUAL ABSTRACT

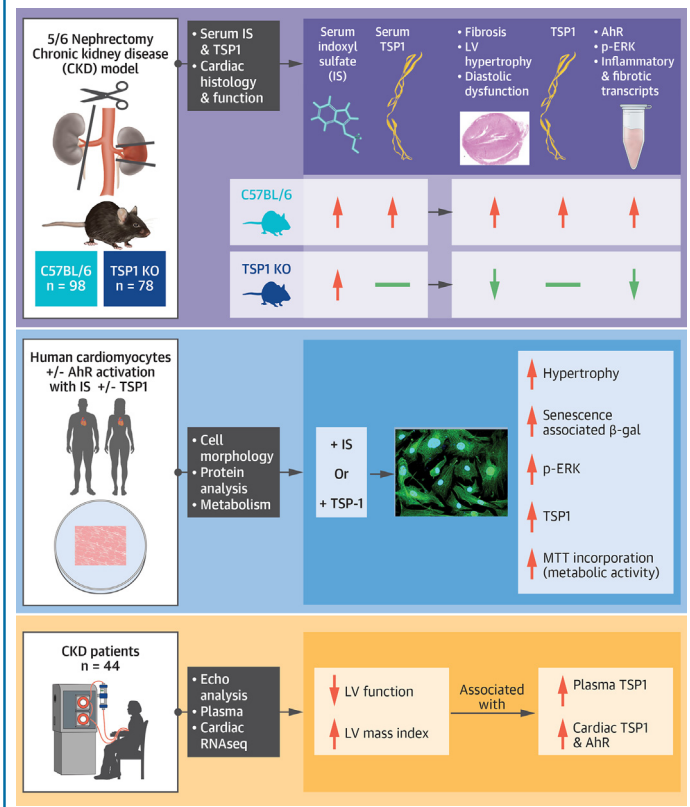

Julovi SM, et al. J Am Coll Cardiol Basic Trans Science. 2024;9(5):607-627.

HIGHLIGHTS

- **CRS type 4 is characterized by CKD, cardiac fibrosis, LVH, and diastolic dysfunction, which can lead to HF.**
- **The uremic toxin IS disrupts cellular and molecular pathways in both CKD and CVDs.**
- **The matricellular protein TSP1 is known to be elevated in patients with CKD and the disruption of TSP1 signaling provides cardioprotection in preclinical studies.**
- **For the first time, this study has identified the role of TSP1 as a mediator of cardiac fibrosis, LVH, and diastolic dysfunction in CKD, as well as its link to IS.**
- **Further studies are required in large clinical studies to confirm the translational role of TSP1 in patients with CKD.**

From the [a]Kidney Injury Group, Centre for Transplant and Renal Research, Westmead Institute for Medical Research, Westmead, New South Wales, Australia; [b]Faculty of Medicine and Health, The University of Sydney, Camperdown, New South Wales, Australia; [c]Sydney Precision Data Science Centre, University of Sydney, New South Wales, Australia; [d]Tissue Pathology and Diagnostic Oncology, Institute of Clinical Pathology and Medical Research, Westmead Hospital, Westmead, New South Wales, Australia; [e]School of Mathematics, University of Sydney, New South Wales, Australia; [f]Laboratory of Data Discovery for Health Limited (D24H), Science Park, Hong Kong Special Administrative Region, China; [g]Molecular and Clinical Sciences Research Institute, St George's University of London, London, United Kingdom; [h]Cardiovascular Pathophysiology and Therapeutics Research Group, Basil Hetzel Institute, Woodville, South Australia, Australia; [i]Department of Medicine, The University of Adelaide, Adelaide, South Australia, Australia; and the [j]Renal and Transplantation Unit, Westmead Hospital, New South Wales, Australia.

ISSN 2452-302X https://doi.org/10.1016/j.jacbts.2024.01.010

JACC: BASIC TO TRANSLATIONAL SCIENCE VOL. 9, NO. 5, 2024
MAY 2024:607–627

ABBREVIATIONS AND ACRONYMS

5/6Nx = 5/6 nephrectomy

AhR = aryl hydrocarbon receptor

CKD = chronic kidney disease

CRS = cardiorenal syndrome

CVD = cardiovascular disease

DEG = differentially expressed gene

EF = ejection fraction

ERK = extracellular signal-related protein kinase

HF = heart failure

HFpEF = heart failure with preserved ejection fraction

HCM = human cardiomyocyte

IS = indoxyl sulfate

LV = left ventricular

LVH = left ventricular hypertrophy

MAPK = mitogen activated protein kinase

MHC = myosin heavy chain

MTT = 3-(4,5-dimethylthiazol-2-yl)-2,5-diphenyl-2H-tetrazolium bromide

p = phosphorylated

p53 = tumor protein p53

SASP = senescence-associated secretory phenotype

siRNA = small interfering RNA

TSP1 = thrombospondin 1

TSP1Ab = anti-thrombospondin 1 antibody

TSP1KO = thrombospondin 1 knockout

WT = wild type

SUMMARY

Patients with chronic kidney disease (CKD) face a high risk of cardiovascular disease. Previous studies reported that endogenous thrombospondin 1 (TSP1) involves right ventricular remodeling and dysfunction. Here we show that a murine model of CKD increased myocardial TSP1 expression and produced left ventricular hypertrophy, fibrosis, and dysfunction. TSP1 knockout mice were protected from these features. In vitro, indoxyl sulfate is driving deleterious changes in cardiomyocyte through the TSP1. In patients with CKD, TSP1 and aryl hydrocarbon receptor were both differentially expressed in the myocardium. Our findings summon large clinical studies to confirm the translational role of TSP1 in patients with CKD. (J Am Coll Cardiol Basic Trans Science 2024;9:607–627)

Chronic kidney disease (CKD) is a global public health problem that significantly shortens lifespan primarily by increasing the risk of cardiovascular disease (CVD),[1] particularly manifesting as myocardial ischemia and/or heart failure (HF). Patients with CKD are more likely to die from CVD than progress to end-stage kidney disease, with 50% of deaths due to cardiac events.[2] CKD resulting in chronic HF is known as cardiorenal syndrome (CRS) type 4[3] and has been increasingly identified as a marker of higher morbidity and mortality.[1,4] Left ventricular hypertrophy (LVH) and diastolic dysfunction are the major factors contributing to development of heart failure with preserved ejection fraction (HFpEF) and sudden cardiac death through ischemia and arrhythmia.[5] A linear relationship between worsening glomerular filtration rate and LV function confers poor clinical outcomes and the highest mortality.[6,7]

The molecular pathways that coordinate pathophysiological changes and development of LVH continue to expand and involve mitogen-associated protein kinases ([MAPKs], especially extracellular signaling-related kinase [ERK] 1/2),[8] oxidative stress, and the aryl hydrocarbon receptor (AhR).[9] More recently, cardiac stress has been shown to initiate metabolic alterations in cardiomyocytes that promote senescence, leading to a functional decline that includes hypertrophic growth, β-galactosidase expression, and secretion of proinflammatory cytokines (senescence-associated secretory phenotype [SASP]).[10] A growing body of evidence indicates that uremic toxins represent important, nontraditional cardiovascular risk factors in CKD because they have demonstrable cytotoxic effects,[11] are associated with cardiovascular mortality,[12] and fail to be effectively cleared by dialysis, particularly protein-bound subgroups such as indoxyl sulfate (IS).[13] IS is the best characterized toxin, derived from dietary intake of the essential amino acid tryptophan and converted to indole by the intestinal microbiome. In the absence of effective tubular secretion, serum concentrations are >50× higher in CKD compared to healthy control subjects[12] and are associated with LV dysfunction and cardiovascular mortality.[12,14] Regression of LVH after kidney transplantation and normalization of cardiac parameters suggests that CKD-specific uremia is a primary driver of cardiac pathology.[15] Thrombospondin 1 (TSP1) is a well-characterized extracellular matrix glycoprotein secreted by cells. However, rather than providing structural integrity, it preferentially regulates signaling pathways to alter cell adhesion, proliferation, and viability in response to injury.[16] The cardiac extracellular matrix provides scaffolding for cardiomyocyte attachment, ventricular geometry, and function, which regulates diastolic performance and inflammation.[17] We recently reported induction of right ventricular TSP1 expression in an animal model of pulmonary hypertension and disruption of TSP1 signaling provided protection.[18]

Plasma TSP1 is elevated in patients with CKD;[19] however, the protein did not appear to be derived from fibrotic renal parenchyma. Further work has confirmed high plasma TSP1 concentrations in

The authors attest they are in compliance with human studies committees and animal welfare regulations of the authors' institutions and Food and Drug Administration guidelines, including patient consent where appropriate. For more information, visit the Author Center.

Manuscript received December 11, 2023; revised manuscript received January 29, 2024, accepted January 29, 2024.

dialysis-dependent patients with CRS compared to those without, and levels were predictive of cardiovascular mortality.[14] However, little is known about the specific effects of TSP1 on the LV or cardiomyocytes in the context of CKD. We now implicate TSP1 in a mouse model of CRS, where the hypertrophied LV is a significant source of TSP1 expression, accompanied by oxidative stress, fibrosis, and SASP. These findings were mitigated in thrombospondin-1 knockout (TSP1KO) mice. In vitro we demonstrate a direct relationship of IS, induction of TSP1, and AhR activation in cardiomyocytes that drives hypertrophy and SASP, highlighting this pathway as a driver of uremic cardiomyopathy.

METHODS

ANIMALS. TSP1KO (B6.129S2-$^{Thbs1tm1Hyn/J}$) mice on a C57BL/6J background (back-crossed for 15 generations) were originally purchased from the Jackson Laboratory and were maintained by Australian BioResources. Age-matched (6-8 weeks) male littermate control (wild-type [WT]) and (homozygous) TSP1KO mice were transferred to Westmead Institute for Medical Research, housed, and acclimatized for 2 weeks in the biological facility under a 12-hour light/dark cycle with access to standard chow and water ad libitum under approved protocols (no. 4281 Western Sydney Local Health District and no. 1594 University of Sydney). All animal studies were performed in accordance with the Australian code for the care and use of animals for scientific purposes developed by the National Health and Medical Research Council.

CRS MODEL USING 5/6NX. In this study, 156 mice were used, including 98 WT mice and 58 TSP1KO mice (Supplemental Table 1). Age-matched (8- to 10-week-old) male mice were randomly assigned to sham and 5/6 nephrectomy (5/6Nx) groups. The 5/6Nx model is characterized by high mortality.[20] We altered the conventional method of nephrectomy,[21] which significantly reduced mortality to 10% to ~15% (Supplemental Figure 1A). Animals were anesthetized with isoflurane and oxygen, the left kidney exposed and exteriorized through a left flank subcostal incision, and connective tissue and adrenal gland separated by using normal saline-soaked cotton bud instead of iris scissors to prevent the injury to renal pedicle.[21] The upper and lower renal poles were removed using iris scissors. Hemostasis was achieved with direct pressure, the kidney returned to the abdomen, and the incision closed with 5/0 monofilament nylon. At day 8 following the initial surgery, a right total nephrectomy was performed through a separate flank incision. In sham-operated mice, the kidneys were exposed in 2 separate surgeries but not resected, as described previously.[19,21] Among 108 mice receiving 5/6Nx, 25 were euthanized (mostly on the second postoperative day) owing to illness and/or >25% body weight loss and were excluded from analysis (Supplemental Table 1). Additional data were also excluded in some experiments because of histological artifact, poor resolution of echocardiography images, or an insufficient quantity of serum/urine specimens collected.

Body weight and blood pressure using the tail-cuff plethysmography (CODA machine, Kent Scientific Corporation) were measured weekly.[21] In some experiments, mice were euthanized at week 2 or 6, and tissues were harvested as illustrated in the study design (Supplemental Figure 1B). Metabolic caging was performed at week 10 before transferring to Sydney Imaging Facility at the Charles Perkins Centre for an additional 2 weeks of acclimatization and echocardiography. At week 12, echocardiography was performed (Vevo 2100 Echocardiography Imaging System, VisualSonics), and then mice were euthanized. Heart and wet lung weights were recorded along with tibial length. Organs, plasma, and urine were then processed for analysis and stored at −80 °C. The estimated percentage of removed kidney was calculated by following formula: percentage of removed kidney = weight of excised kidneys (left excised kidney + right kidney) × 100 / total weight of 2 kidneys (left excised + left remnant + right kidney), as described in our recent report.[21]

ASSESSMENT OF RENAL FUNCTION AND PROTEINURIA. Blood urea nitrogen and creatinine, alkaline phosphatase, serum calcium, urinary protein, and creatinine were determined using the Siemens Atellica System (Westmead Hospital).

ENZYME-LINKED IMMUNOSORBENT ASSAY. Mouse plasma IS was measured by enzyme-linked immunosorbent assay according to manufacturer protocol (#MBS720905, MyBioSource, Inc). Briefly, kit contents and samples were brought to room temperature. One hundred microliters (100 μL) of IS standards or samples were added to the enzyme-linked immunosorbent assay plate in duplicate and incubated at 37 °C for 1 hour. The plate was washed 5× with buffer, followed by the addition of conjugate and incubation at 37 °C for 20 minutes. Following addition of stop solution, the plate was read at 450 nm.

HIGH-FREQUENCY ULTRASOUND ECHOCARDIOGRAPHY. Animals were assessed at week 12 under general anesthesia induced with isoflurane and O_2 titrated to effect. Animals were placed supine on an adjustable stage with the tail of the animal facing toward

FIGURE 1 Development of CKD in WT and TSP1KO Mice

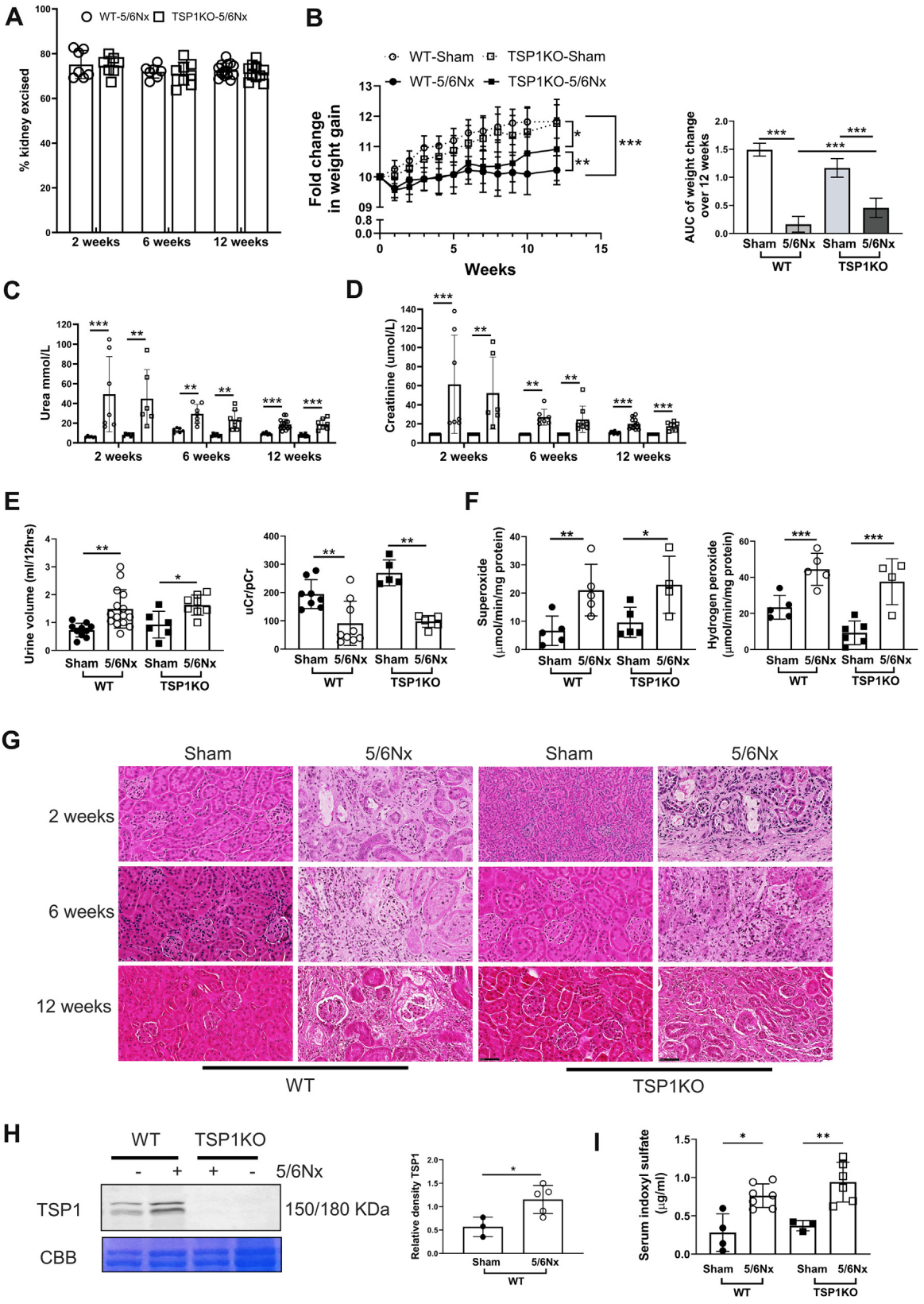

Continued on the next page

the operator and limbs secured to electrocardiogram probes. The Vevo2100 ultrasound system (VisualSonics) and linear transducer (MS550D, MicroScan, 40 MHz, VisualSonics) were used to acquire LV parasternal long-axis B-mode/echocardiogram-gated kilohertz visualization images and short-axis mid-papillary echocardiogram-gated kilohertz visualization/M-mode images. Pulse-wave and tissue Doppler images were obtained in apical 4-chamber view using a linear transducer 57 MHz (VevoF2, VisualSonics) as previously described.[22] All images were acquired by an operator blinded to the treatment group. Short-axis mid-papillary M-mode analyses (Supplemental Figure 1C) were carried by selecting autoLV from 3 cycles of each cine loop. Pulse-wave and tissue Doppler images (Supplemental Figures 1D and 1E) analyses were carried out to measure diastolic (dys)function. VevoLAB software (VisualSonics) was used for data analysis, and average data from 3 cine loops are presented for each mouse.

HEART HISTOPATHOLOGY. Formalin-fixed kidney and heart tissue embedded in paraffin were sectioned at 4 μm and stained with hematoxylin and eosin or picrosirius red using standard methods.[19,21] Slides were viewed under brightfield conditions. Picrosirius red staining area and intensity were measured and quantified using ImageJ (National Institutes of Health) as previously described.[19] Picrosirius red stained images (magnified 80×) were also used to measure the cross-sectional area of cardiomyocytes using ImageJ. Assessors were blinded to treatment groups.

CELL CULTURE. Human primary cardiomyocytes (PromoCell) were subcultured according to manufacturer's instructions. Cells were used at passages 3-6. Cells at ∼70% confluency in 6-well plates were treated with recombinant human TSP1 (Athens Research and Technology), IS (Sigma Aldrich) for 24 hours. In some experiments, cells were pretreated with anti-TSP1 (#ab85762) and sarcomeric (#ab68167) antibodies were from Abcam at 1 μg/mL or mouse immunoglobulin G_1 isotype control (#02-6100, Invitrogen) prior to treatment. For small interfering RNA (siRNA) experiments, cells were plated in media without antibiotics and transfection performed at 50%-60% confluence using Lipofectamine 2000 and TSP1 or control siRNA (Invitrogen) in Opti-MEM (Thermo Fisher Scientific) according to the manufacturer's instructions. Cells were exposed to siRNA for 48 hours prior to experimental use.

Human aortic vascular smooth muscle cells (Clonetics, Lonza) were used in subsequent experimental work owing to the unavailability of human cardiomyocytes (HCMs) in Australia. Human aortic vascular smooth muscle cells were subcultured according to manufacturer's instructions to detect the involvement of AhR in IS-induced TSP1 expression. Cells were used among passages 3-6. For this experiment, cells were pretreated with AhR inhibitor (StemRegenin 1, ab142174, Abcam) (10 μmol/L) for 2 hours and then treated with IS (10 μmol/L) for 24 hours.

Human cardiac fibroblasts (Lonza) were subcultured according to manufacturer's instructions. Cells were used among passages 4-8. Cells at ∼70% confluency were treated with recombinant human TSP1 (Athens Research and Technology) for 24 hours.

Cell viability and senescence assays. Cell metabolic activity was measured using a XTT Cell Viability Kit (Cell Signaling Technology), and senescence was assessed with a Mammalian β-Galactosidase Assay Kit (Thermo Fisher Scientific). Briefly, 10^4 cells/well were seeded into a 96-well microplate. Serum-starved cells were treated with TSP1 (0.2-10.0 nmol/L) or IS (1-500 μmol/L) for 48 hours. Cell proliferation and senescence were determined at the 450 nm and 405 nm, respectively, using Proteomics SpectraMax iD5 Plate Reader (VWR International).

Cells were stained using a Senescence-β-Galactosidase Staining Kit (Cell Signaling Technology) according to manufacturer's instructions. Samples were then washed in phosphate-buffered saline, and images were captured at random using a light

FIGURE 1 Continued

Wild-type (WT) and thrombospondin-1 knockout (TSP1KO) mice were subjected to sham surgery or 5/6-nephrectomy (5/6Nx). (A) Percentage of kidney excised following 5/6Nx at 2, 6, and 12 weeks (n = 7-13). (B) Fold change in body weight over 12 weeks (n = 6-21). Serum urea (C) and serum creatinine (D) at 2, 6, and 12 weeks (n = 6-14), and (E) urine volume and urinary/plasma creatinine ratios (uCr/pCr) at 10 weeks (n = 5-15). (F) Detection of superoxide and H_2O_2 moieties in WT and TSP1KO kidney homogenates (n = 4-6). (G) Representative hematoxylin and eosin-stained kidney histology (bar = 50 μm). (H) Expression of plasma TSP1 by Western blotting in sham-operated and 5/6Nx mice. The band density of the protein is normalized with Coomassie brilliant blue (CBB) and combined densitometries are shown (n = 3-5). (I) Serum indoxyl sulfate at week 12 was detected by enzyme-linked immunosorbent assay (n = 3-6). All data are mean ± SD. $*P < 0.05$, $**P < 0.01$, and $***P < 0.001$ by 2-way analysis of variance with Tukey post hoc test (A to F [at each time point], I), and the representing graph (H) was analyzed by unpaired Student's *t*-test. AUC = area under the curve; CKD = chronic kidney disease.

FIGURE 2 **CKD in Mice Induces TSP1-dependent LVH**

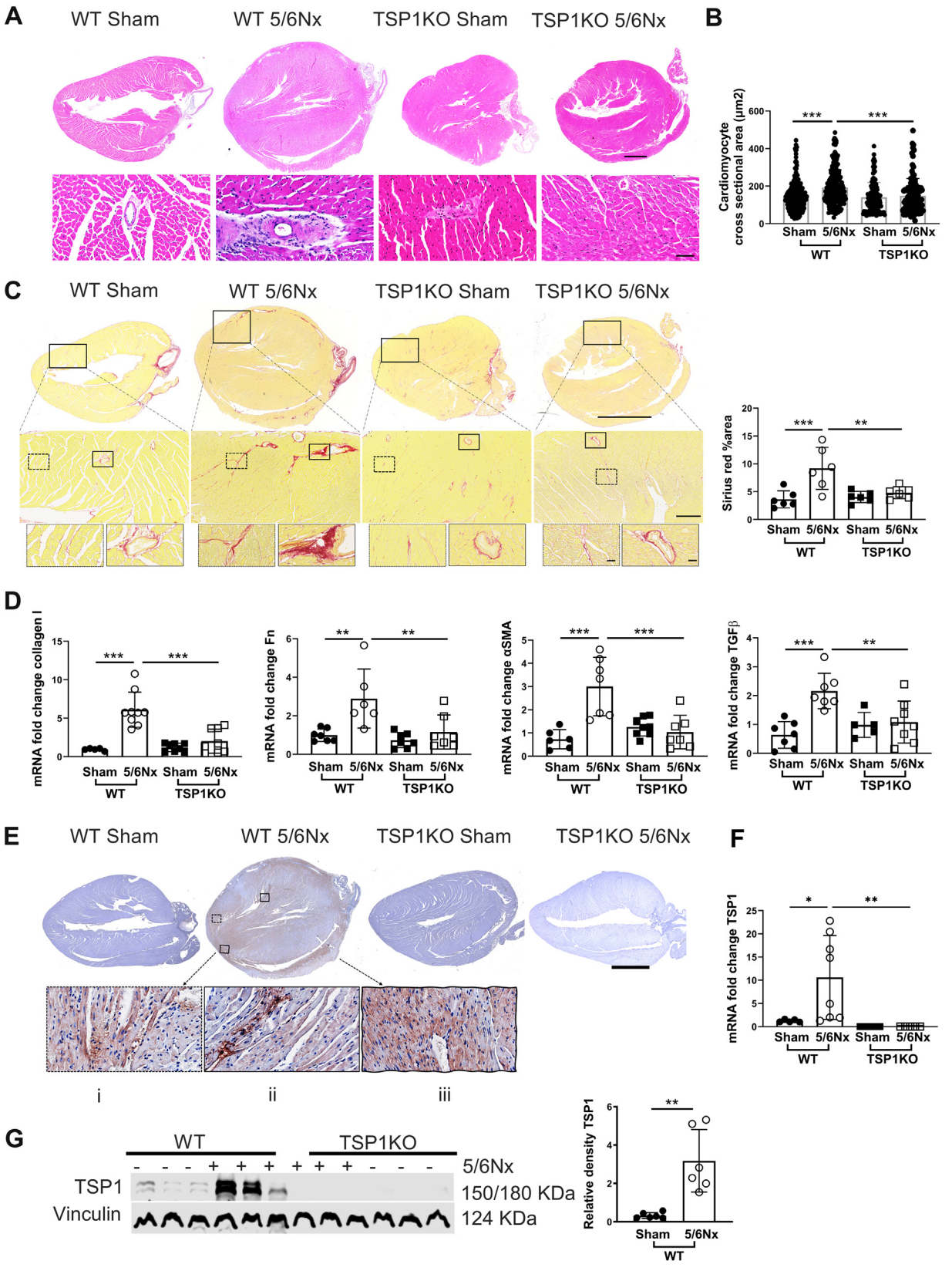

Continued on the next page

microscope (CKX41, Olympus). At least 5 images were captured from each well and blindly assessed for senescence-associated β-galactosidase (blue)-positive cells.

WESTERN BLOTTING. Tissue or cells were homogenized in cold radio immunoprecipitation assay buffer (Cell Signaling Technology) that contained protease inhibitor cocktail (Sigma-Aldrich) and phosphatase inhibitor cocktail (Roche Applied Science). Protein was quantified using a DC assay (BioRad), resolved by sodium dodecyl sulfate polyacrylamide gel electrophoresis and then transferred onto nitrocellulose membranes (BioRad). Blots were probed at 4 °C overnight with the following primary antibodies: phospho-p44/42 MAPK (pERK1/2) (#4370), p44/42 MAPK (ERK1/2) (#9107), tumor protein p53 (p53) (#2524), $p21^{Waf1/Cip1}$ (#64016), $p27^{Kip1}$ (#3698), AhR (#83200), vinculin (#13901), and β-actin (#4970) all from Cell Signaling Technology. TSP1 (#ab85762), sarcomeric α-actinin (#ab68167) were from Abcam. Atrial natriuretic peptide (#PA5-29559), brain natriuretic protein (#PA5-98294), and cardiac myosin heavy chain (#MA1-26180) were from Invitrogen. Myosin heavy chain (MHC)-β (#sc-53089) was from Santa Cruz Biotechnology. Protein was visualized on an Odyssey LCx Imaging System (Licor). Expression was normalized to the levels of total protein loading or housekeeping gene. Protein band intensity was evaluated using ImageJ.

RNA EXTRACTION AND QUANTIFICATION BY REAL-TIME QUANTITATIVE POLYMERASE CHAIN REACTION. RNA was extracted using ISOLATE-II RNA MiniKits (Bioline) with on-column DNase treatment. RNA was quantified using a Nanodrop (BioTek) and reverse-transcribed using a SensiFAST cDNA synthesis kit (Bioline). Complementary DNA was amplified in triplicate with commercially available gene-specific primers (Invitrogen) using a CFX384 PCR machine (BioRad). Thermal cycling conditions were 95 °C for 2 minutes, followed by 40 cycles of 95 °C for 10 seconds and 60 °C for 30 seconds. Data were analyzed using the ΔΔCt (cycle threshold) method with expression normalized to the housekeeping gene and sham-operated WT animals/control cells used as referent control animals/cells.

IMMUNOHISTOCHEMISTRY. Immunostaining was performed as previously described.[19,21] Four-micrometer sections of paraffin-embedded mouse heart tissues were incubated with TSP1 (Abcam), AhR (#LS-B4900, LSBio) or isotype-matched immunoglobulin G. For immunodetection, Dako EnVision+ System-HRP labeled polymer detection kit (Dako) was used with ImmPACT NovaRED Peroxidase (HRP) Substrate (Vector Laboratories) and counterstained by Mayer hematoxylin and Scott bluing solution. After mounting, slides were viewed by Nano Zoomer (Hamamatsu). All samples were stained, imaged, and analyzed simultaneously to exclude between-run variability. AhR staining intensity was calculated from the 5 randomly selected areas at 10× magnification, as published previously.[23]

REACTIVE OXYGEN SPECIES CHARACTERIZATION. Measurement of superoxide ($O_2^{\bullet -}$) and H_2O_2 was performed using cytochrome c and Amplex Red assays, respectively, as published previously.[24,25] Tissues were homogenized in lysis buffer and centrifuged at 1,000*g*; membranes were resuspended in lysis buffer; and protein concentration was measured using the Bradford microplate method. $O_2^{\bullet -}$ production was initiated by the addition of 180 μmol/L nicotinamide adenine dinucleotide phosphate hydrogen and was calculated from the initial linear rate of superoxide dismutase (150 U/mL)-inhibitable cytochrome c reduction quantified at 550 nm and using an extinction coefficient of 21.1 $mmol/L^{-1}\ cm^{-1}$ (BioTek Synergy 4 Hybrid Multi-Mode Microplate Reader). To detect H_2O_2, protein was added to the wells containing the assay

FIGURE 2 Continued

(A) Representative left ventricle hematoxylin and eosin–stained histology (bars = 1 mm [top panel] and 50 μm [bottom panel]) and (B) cross-sectional surface area of individual cardiomyocytes. Measurements are from randomly chosen cells (n = 310 WT-sham, 279 WT-5/6Nx, 298 TSP1KO-sham, 214 TSP1KO-Nx) from 4 mice. Regions of interest at the margin of images or incomplete regions of interest were excluded from the counting. (C) Representative left ventricular picrosirius red staining with accompanying histogram of staining area from 5 independent fields of view (n = 6) (bars = 2.5 mm [top], 250 μm [middle], and 25 μm [bottom]). (D) Left ventricular messenger RNA (mRNA) expression of fibrosis markers collagen 1, fibronectin (Fn), α-smooth muscle actin (SMA), and TGF-β by quantitative polymerase chain reaction, normalized to HPRT1 with WT sham-operated left ventricle set as the referent control (n = 6-7). (E) Representative left ventricular immunohistochemical staining for TSP1 (bar = 2.5 mm) with high magnification areas (bars = 50 μm): (i) injured area, (ii) interstitial space, and (iii) cardiomyocytes. (F) Left ventricular mRNA expression of TSP1 by quantitative polymerase chain reaction, normalized to HPRT1 with WT sham-operated left ventricle set as the referent control (n = 5-8). (G) Left ventricular homogenates were analyzed for TSP1 expression by Western blotting. Band density was normalized with vinculin and combined densitometries are shown (n = 6). All data are mean ± SD; $^*P < 0.05$, $^{**}P < 0.01$, and $^{***}P < 0.001$ by 2-way analysis of variance with Tukey post hoc test (A to D) or unpaired Student's *t*-test (G). HPRT1 = hypoxanthine phosphoribosyltransferase 1; LVH = left ventricular hypertrophy; other abbreviations as in Figure 1.

FIGURE 3 **CKD in Mice Promotes Cardiac Hypertrophy and Senescence via TSP1**

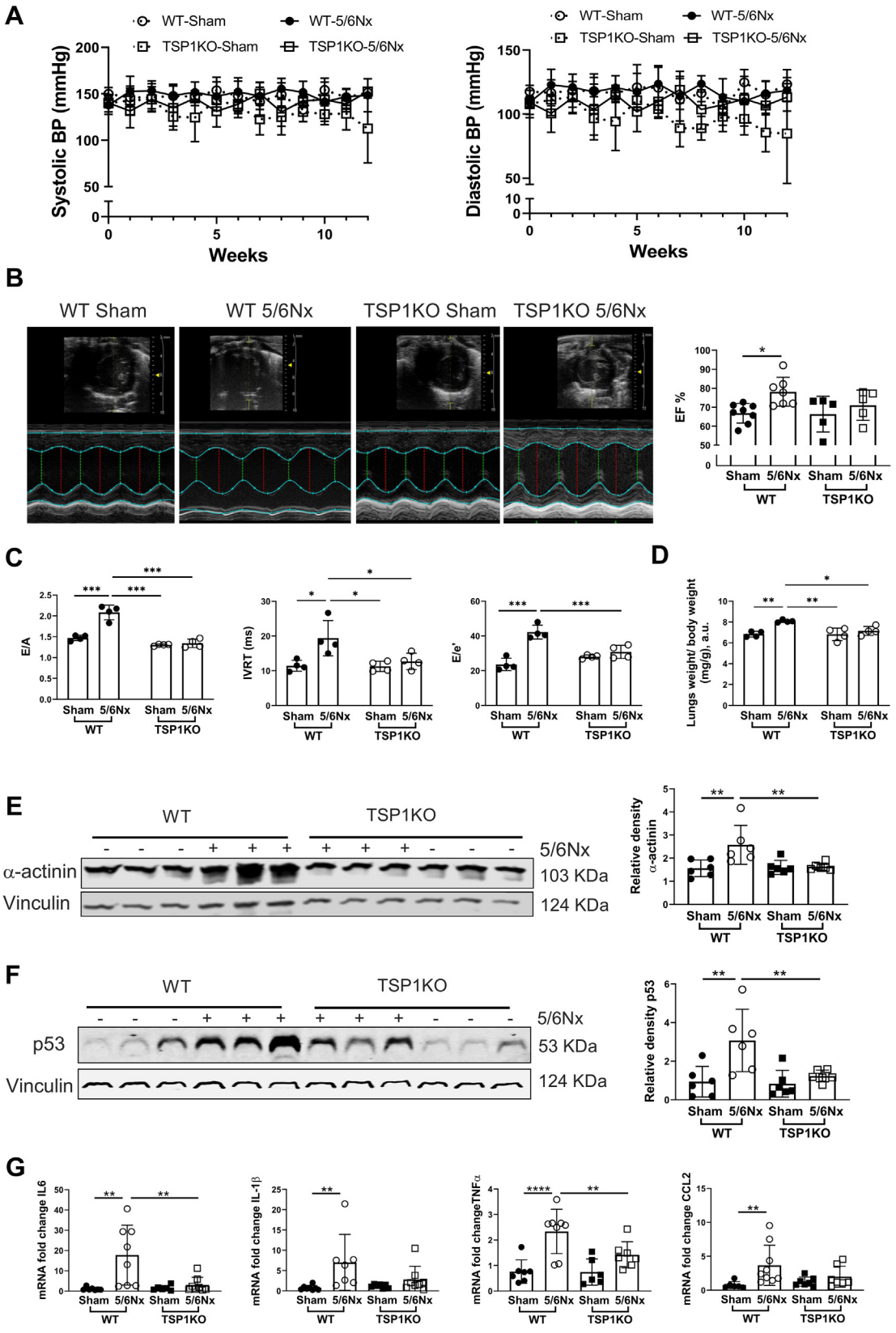

Continued on the next page

mixture, and the reaction was initiated by the addition of 36 μmol/L nicotinamide adenine dinucleotide phosphate hydrogen. Fluorescence was detected using the BioTek Synergy 4 Hybrid Multi-Mode Microplate Reader with a 530/25 excitation and a 590/35 emission filter. The reaction was monitored for 30 minutes at 25 °C. To confirm the H_2O_2 signal, catalase (300 U/mL) was added in parallel wells, and the catalase-inhibitable rate of H_2O_2 production was quantified from a H_2O_2 standard curve.

HUMAN DATA. The raw expression data were accessed form the Gene Expression Omnibus using the accession code GSE160145 and imported into R version 4.2.0 (R Foundation).[26] The raw reads were normalized using DESeq's Median of Ratios method and variance stabilization transformation performed using the DESeq2 package in R. Differential genes were identified between patients listed with CKD and healthy patients. Genes with a log-fold change >2, and an adjusted $P < 0.05$ using the Benjamini-Hochberg false discovery rate were determined to be differentially expressed. A Wilcoxon rank-sum test was used to identify enriched Kyoto Encyclopedia of Genes and Genomes pathways[27] between healthy and patients with CKD. Gene Set Enrichment Analyses was executed using the clusterProfiler package in R[28] on the list of differentially expressed genes (DEGs) between healthy and patients with CKD using Gene Ontology pathway database.[29] Data used for this study are publicly available using the Gene Expression Omnibus accession code listed. The code used to generate analysis and figures is available online.[30] No other clinical data or demographics were available for this patient cohort.

HUMAN PLASMA TSP1 AND ECHOCARDIOGRAPHY CORRELATION. The study was approved by the Human Research Ethics Committee of Western Sydney Local Health District (HREC LNR/12/WMEAD/114 and LNRSSA/12/WMEAD/117 [3503]). In brief, patients were recruited from nephrology outpatient clinics at Westmead Hospital and did not have an intercurrent illness. All subjects were previously recruited, and their plasma TSP1 levels were measured and published.[19] Patients with echocardiography studies within 3 months of venopuncture and not associated with acute illness or cardiovascular deterioration were used for analysis.

STATISTICAL ANALYSIS. Statistical analyses were performed using GraphPad Prism software (version 10.0.3; GraphPad Software Inc). Data are presented as mean ± SD or median (25th, 75th percentiles) (box plot) dependent on data distribution. Between-group comparisons used unpaired Student's *t*-test or Wilcoxon rank-sum test, whereas within-group comparisons used paired Student's *t*-tests. One- or 2-way analysis of variance was used to compare >2 groups with Sidak's or Tukey's post hoc test for multiple pairwise comparisons. Spearman's correlation coefficient (*r*) was used to evaluate the association of 2 continuous variables as determined through linear regression. Kaplan-Meier methods were used to present survival curves with groups compared using the log-rank test. A value of $P < 0.05$ was considered statistically significant.

RESULTS

DEVELOPMENT OF EQUIVALENT CKD IN WT AND TSP1KO MICE. A 5/6Nx model recapitulates features of CKD and induces cardiac remodeling. Removal of 70%-80% of total kidney mass at multiple time points (**Figure 1A**) demonstrated reduced body weight in WT- and TSP1KO-5/6Nx mice compared to sham-operated control mice, although weight reduction was less in TSP1KO-5/6Nx mice compared to WT-5/6Nx mice (**Figure 1B**). Acute elevation of serum urea and creatinine was seen at 2 weeks post-5/6Nx (**Figures 1C and 1D**), which reduced with time. Serum urea, serum creatinine, polyuria, and decreased urine creatinine/plasma creatinine ratio was equivalent in both genotypes post-5/6Nx (**Figures 1C to 1E**). TSP1 is a well-recognized activator of oxidative stress,[23] but

FIGURE 3 Continued

Systolic and diastolic blood pressure (BP) using tail-cuff plethysmography over 12 weeks in WT or TSP1KO mice following 5/6Nx or sham operation (n = 20-23). (B) Representative images of left ventricle echocardiography and measurement of ejection fraction (EF) at 12 weeks (n = 5-8). (C) Four apical view echocardiography analysis. E/A ratio of early mitral flow velocity (E) and late diastolic transmitral flow velocity (A), isovolumic relaxation time (IVRT), and E/e′ ratio of early mitral flow velocity (E) and diastolic septal mitral annulus velocity (e′) (n = 4). (D) Lung weight normalized by the tibial length (n = 4). Mice left ventricular homogenates were analyzed by Western blotting for expression of (E) α-actinin, and (F) senescence markers tumor protein p53 (p53). Band density was normalized with vinculin and combined densitometries were shown (n = 6). (G) Left ventricular messenger RNA expression of senescence-associated secretory phenotype cytokines interleukin (IL)-6, IL-1β, TNF-α, and CCL2 by quantitative polymerase chain reaction, normalized to HPRT1 with WT sham-operated left ventricle set as the referent control (n = 6-9). All data are mean ± SD; *$P < 0.05$, **$P < 0.01$, and ***$P < 0.001$ by 2-way analysis of variance with Tukey post hoc test. a.u. = arbitrary units; other abbreviations as in **Figure 1**.

FIGURE 4 CKD in Mice Promotes Cardiac Oxidative Stress, Inflammation, and MAPK Up-Regulation via TSP1

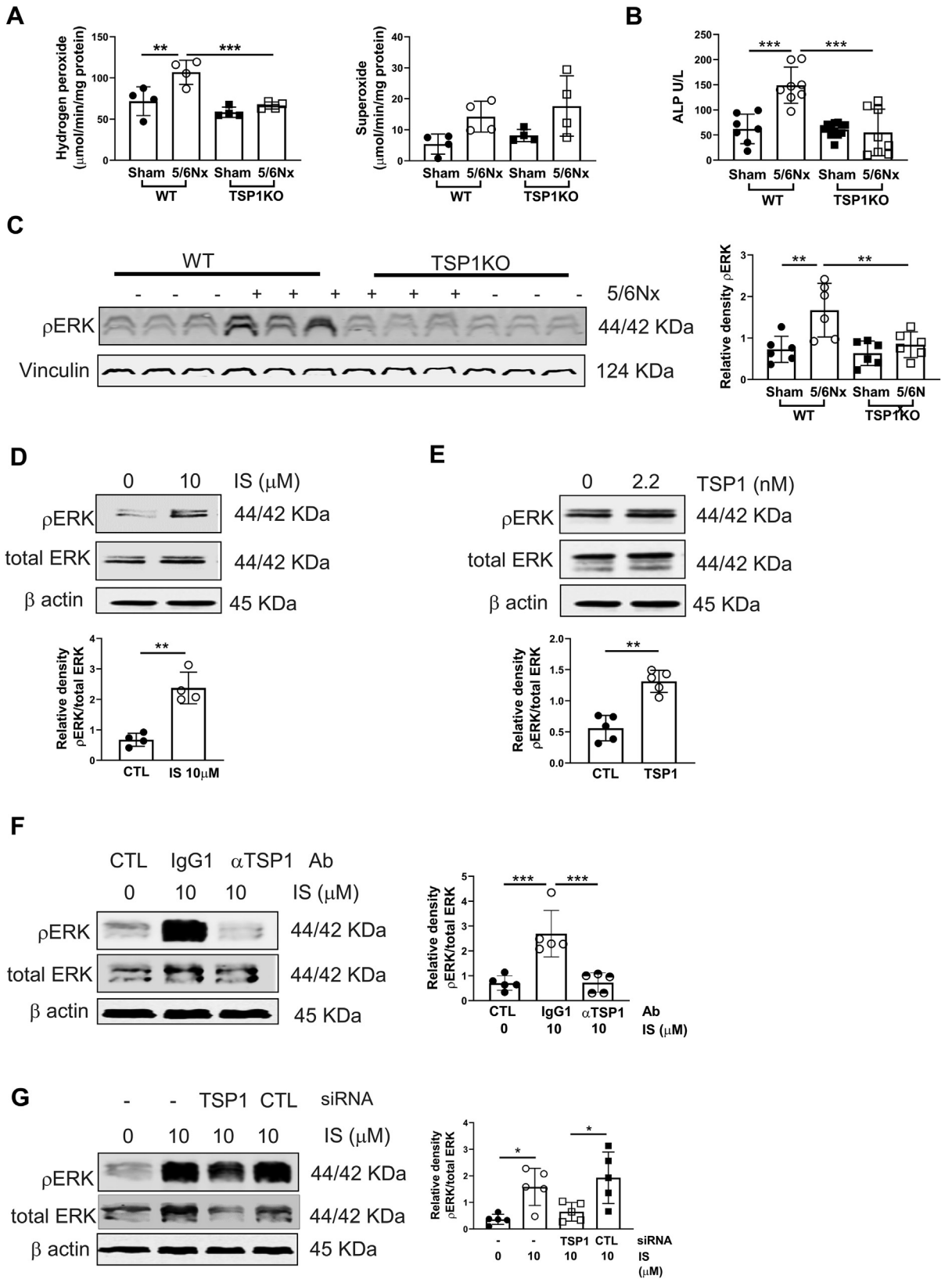

Continued on the next page

there were no differences in reactive oxygen species in the remnant kidney of WT- and TSP1KO-5/6Nx mice (**Figure 1F**). Photomicrographs of the remnant kidney over time are demonstrated in **Figure 1G**. At 12 weeks following 5/6Nx, the renal parenchyma demonstrated fibrosis and tubular atrophy in addition to changes in glomerular morphology that included tuft shrinkage and glomerulosclerosis in both genotypes (**Figure 1G**). Plasma TSP1 was up-regulated only in WT-5/6Nx mice (**Figure 1H**). As expected, plasma IS was up-regulated in WT-5/6Nx and TSP1KO-5/6Nx mice compared to WT-sham and TSP1KO-sham mice, respectively (**Figure 1I**).

GENETIC DISRUPTION OF TSP1 SIGNALING LIMITS CARDIAC PATHOLOGY IN A MOUSE MODEL OF CRS. Given equivalent renal dysfunction between WT- and TSP1KO-5/6Nx mice, we then explored changes in cardiac phenotype. Representative sections demonstrated LVH (**Figure 2A**) and increased cardiomyocyte cross-sectional area only in WT-5/6Nx mice (**Figure 2B**, Supplemental Figure 2A), accompanied by increased heart weight (compared to tibial length) (Supplemental Figure 2B). Perivascular and interstitial fibrosis was demonstrated in WT-5/6Nx hearts (**Figure 2C**), which was corroborated by significantly elevated collagen I, fibronectin, α-smooth muscle actin, and transforming growth factor-β (**Figure 2D**). LVH and fibrosis were abrogated in TSP1KO-5/6Nx hearts. Immunohistochemical staining revealed marked myocardial TSP1 expression, localized to the cardiomyocytes and interstitial, vascular, and perivascular spaces only in WT-5/6Nx mice (**Figure 2E**, Supplemental Figure 2C), confirmed by quantitative polymerase chain reaction (**Figure 2F**) and Western blotting (**Figure 2G**) of LV tissue.

TSP1 IS REQUIRED TO PROMOTE LVH, DIASTOLIC DYSFUNCTION, AND SENESCENCE IN MICE WITH CRS. Systolic and diastolic pressure and mean arterial pressure and heart rate were not statistically significantly lower in TSP1KO mice compared to WT mice (**Figure 3A**, Supplemental Figure 2D). Echocardiography performed at week 12 confirmed the histological evidence of LVH, with increased EF and fractional shortening exclusively in WT-5/6Nx mice (**Figure 3B**, Supplemental Figure 2E). Consistent with previous reporting,[31] this was accompanied by decreased LV systolic internal diameter and systolic volume (Supplemental Figure 2F). LV diastolic internal diameter and volume were preserved in TSP1KO-5/6Nx mice (Supplemental Figure 2G).

Diastolic dysfunction frequently correlates with heightened interstitial fibrosis, concentric hypertrophy, and atrial enlargement. The early flow velocity (E) of the mitral valve exhibited no significant variance among the groups (Supplemental Figure 3A). Doppler assessment of LV filling velocity, determined by the ratio of early (E) to late (A) diastolic transmitral Doppler flow velocities (E/A), and isovolumetric relaxation time was significantly increased in WT-5/6Nx mice compared to sham-operated mice, but not in TSP1KO-5/6Nx mice (**Figure 3C**).

The septal mitral annular velocity (e′) demonstrated a significant reduction in WT-5/6Nx, TSP1KO sham, and TSP1KO-5/6Nx mice when compared to WT-sham mice (Supplemental Figure 3B). Moreover, the E/e′ ratio was significantly increased solely in WT-5/6Nx mice (**Figure 3C**), indicating the onset of diastolic dysfunction, with no such elevation observed in TSP1KO-5/6Nx mice. Furthermore, lung weight was increased in WT-5/6Nx mice (**Figure 3D**), which is suggestive of increased lung congestion and HFpEF.

LVH increases cardiomyocyte contractile machinery[32] that is governed by overexpression of MHC and α-actinin, which provide adenosine triphosphate hydrolysis[33] and anchor actin filaments to the sarcomeric Z-disk,[34] respectively. WT-5/6Nx hearts demonstrated significantly up-regulated α-actinin

FIGURE 4 Continued

Measurement of (A) superoxide and H_2O_2 (n = 4) in left ventricular tissue, and (B) serum alkaline phosphatase (ALP) (n = 7-12). (C) Expression of phosphorylated extracellular regulated kinase (pERK), and vinculin by Western blotting in the left ventricle from WT or TSP1KO hearts following 5/6Nx or sham operation (n = 6). Band density was normalized with vinculin. (D,E) Human cardiomyocyte cells at ∼70% confluence in 6-well plates were treated with indoxyl sulfate (IS) (10 μmol/L) (D, n = 4) and TSP1 (2.2 nmol/L) (E, n = 5) for 24 hours. pERK and total ERK were measured by Western blotting in whole-cell lysates. β-actin was used as an internal control. (F) Human cardiomyocyte cells were pretreated treated with immunoglobulin G_1 (IgG_1) (1 μg/mL) or anti-TSP1 antibody (αTSP1Ab) (1 μg/mL) for 2 hours and then treated with IS (10 μmol/L) for 24 hours. pERK and total ERK were measured by Western blotting in whole-cell lysates. β-actin was used as an internal control (n = 5). (G) Human cardiomyocyte cells were pretreated with control (CTL) siRNA (50 nmol/L) or TSP1small interfering RNA (siRNA) (50 nmol/L) for 48 hours and then treated with IS (10 μmol/L) for 24 hours. pERK and total ERK were measured by Western blotting in whole-cell lysates. β-actin was used as an internal control (n = 5). Band density was normalized with total ERK. Graphs are mean ± SD; *$P < 0.05$, **$P < 0.01$, and ***$P < 0.001$ by 1-way analysis of variance (F to H) and 2-way analysis of variance with Tukey Post hoc test (A to C, F, G) or unpaired Student's *t*-test (D, E). CTRL = control; MAPK = mitogen activated protein kinase; other abbreviations as in **Figure 1**.

FIGURE 5 Myocardial Activation of AhR Is Up-Regulated in CRS

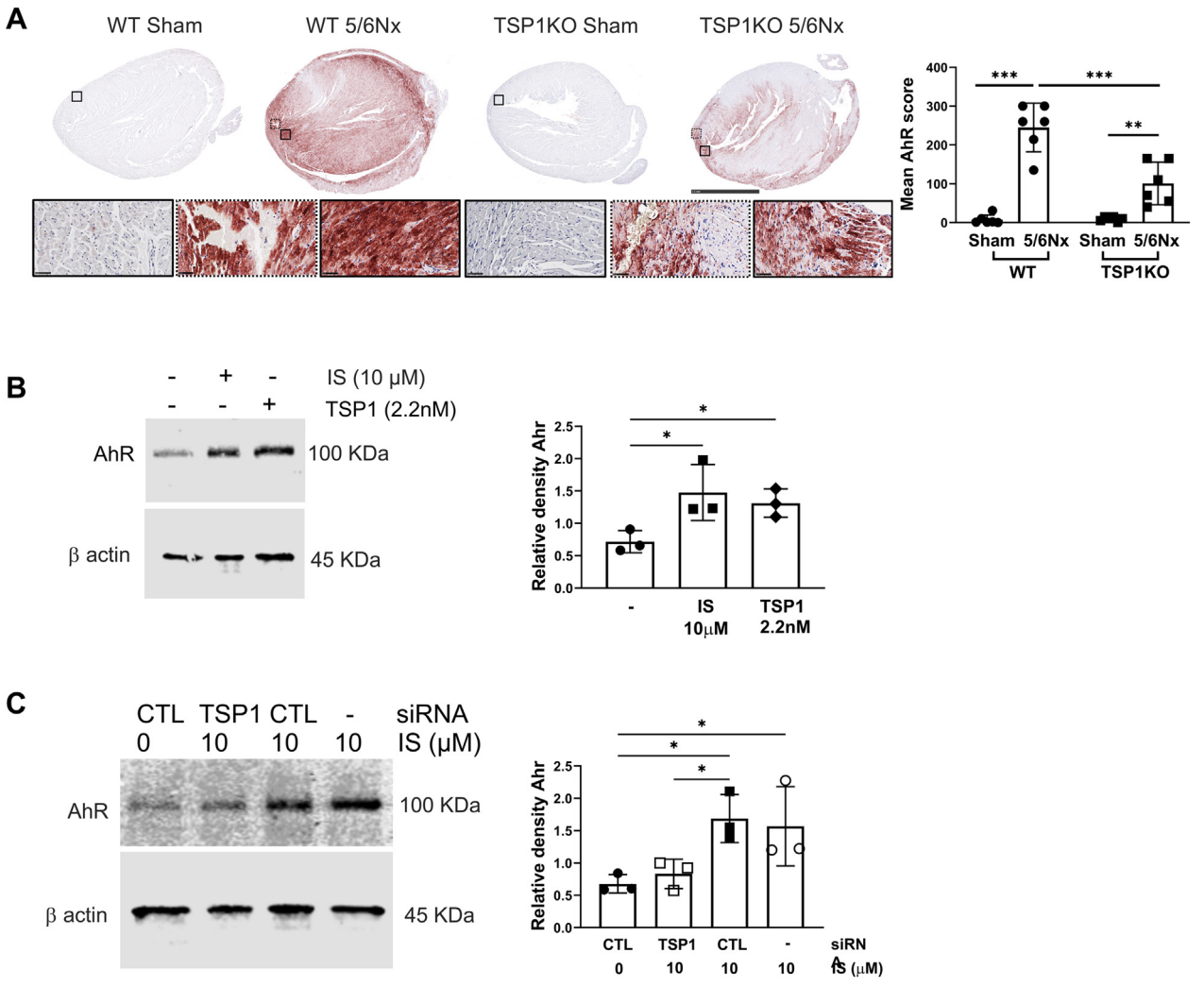

(A) Representative left ventricle immunohistochemical staining for aryl hydrocarbon receptor (AhR) (bar = 2.5 mm) with high magnification areas (bars = 50 μm), with the accompanying histogram of mean AhR scoring (n = 6). (B) Human cardiomyocyte cells at ~70% confluence in 6-well plates were treated with IS (10 μmol/L) or TSP1 (2.2 nmol/L) for 24 hours. AhR was measured by Western blotting in whole-cell lysates. β-actin was used as an internal control (n = 3). (C) Human cardiomyocyte cells were pretreated with CTL (50 nmol/L) or TSP1 siRNA (50 nmol/L) for 48 hours and then treated with IS for 24 hours. AhR was measured by Western blotting in whole-cell lysates. β-actin was used as an internal control (n = 3). Band density was normalized with β-actin. All data are mean ± SD; *$P < 0.05$, **$P < 0.01$, and ***$P < 0.001$ by 2-way analysis of variance with Tukey post hoc test (A) or 1-way analysis of variance with Sidak multiple comparisons test (B, C). CRS = cardiorenal syndrome; other abbreviations as in Figures 1 and 4.

(Figure 3E) and β- MHC, with reduced α-MHC (Supplemental Figure 3C). Expression of both atrial and brain natriuretic peptides was elevated in WT-5/6Nx mice compared to TSP1KO-5/6Nx mice, with no difference in α-MHC expression (Supplemental Figure 3C). WT-5/6Nx hearts also showed amplified expression of senescence markers p53, $p21^{cip}$, and $p27^{kip1}$ (Figure 3F, Supplemental Figure 3D), which was associated with up-regulated proinflammatory cytokines (Figure 3G). Senescence and proinflammatory markers were mitigated in TSP1KO-5/6Nx mice (Figure 3G).

DISRUPTION OF TSP1 SIGNALING IN MICE WITH CRS MITIGATES LV OXIDATIVE STRESS AND THE MAPK/ERK PATHWAY. Growing evidence implicates redox pathways[35] and chronic inflammation[36] in the development of LVH and contractile dysfunction. WT-5/6Nx

LV tissue demonstrated significantly greater oxidative stress in the form of H_2O_2, which was mitigated in TSP1KO-5/6Nx tissue; superoxide moiety measurements were equivalent (**Figure 4A**). Tissue nonspecific alkaline phosphatase is associated with systemic inflammation[37] and positively correlates with cardiovascular events.[38] WT-5/6Nx mice demonstrated elevated serum alkaline phosphatase, which was abrogated in TSP1KO-5/6Nx animals (**Figure 4B**). Histologic examination also revealed areas of heterotopic ossification only seen in WT-5/6Nx hearts (Supplemental Figure 3E).

Reactive oxygen species and inflammation activate a broad variety of hypertrophy signaling kinases,[39] including MAPK signaling cascades, which are central regulators of pathological LVH.[40] MAPK ERK is also linked to TSP1 activity and H_2O_2availability.[41] pERK expression was up-regulated only in WT-5/6Nx hearts (**Figure 4C**). To demonstrate that this effect could be replicated in vitro, we incubated HCMs with IS or TSP1, and both up-regulated pERK (**Figures 4D and 4E**), which was mitigated with anti-thrombospondin 1 antibody ([αTSP1Ab], which demonstrates direct inhibitory[42] and steric hindrance[43] effects on TSP1 activity) or siRNA (**Figures 4F and 4G**). These data suggest that the effect of IS was dependent on intact TSP1 signaling.

CRS IS ASSOCIATED WITH AhR ACTIVATION. IS is a ligand and potent agonist of AhR, and this interaction is clinically relevant in CKD[44] because it regulates the cell cycle and responsiveness to oxidative stress.[45] AhR regulates TSP1 gene promoter activity,[46] and MAPK activation has also been shown to facilitate AhR activity,[47] suggesting bidirectional potentiation of signaling. Immunohistochemical staining revealed marked myocardial AhR activation in WT-5/6Nx hearts, which was mitigated in TSP1KO-5/6Nx hearts (**Figure 5A**). IS and TSP1 were both capable of up-regulating AhR activation in HCMs (**Figure 5B**), and IS-induced AhR activation was mitigated by TSP1 siRNA (**Figure 5C**). Human vascular smooth muscle cells exposed to an AhR inhibitor demonstrated reduced TSP1 expression, even when concurrently treated with IS (Supplemental Figure 4A), supporting the notion that AhR is required for TSP1 activation. The proinflammatory cytokine profile characteristic of SASP remained intact with induction of TNF-α, interleukin-6, interleukin-1β, and CCL2 with IS, but this was limited in the presence of AhR inhibitors (Supplemental Figure 4B).

IS INDUCES CARDIOMYOCYTE HYPERTROPHY AND SASP MEDIATED BY TSP1. Our global KO mouse did not distinguish which cells were driving LVH in CRS; however, we initially focused on pathologic signaling within cardiomyocytes. We evaluated the response of HCMs to IS and TSP1, demonstrating up-regulation of TSP1 in response to both (**Figure 6A**, Supplemental Figure 5A) at concentrations found in patients with CKD.[48] A positive feedback loop in response to exogenous TSP1 is counterintuitive to cellular response to injury, but this remains a robust observation in other cell types.[18,49] IS-mediated induction of TSP1 was limited by TSP1 siRNA and αTSP1Ab at protein (**Figure 6B**) and transcript levels (**Figure 6C**). Similar to our in vivo findings, α-actinin expression increased with exogenous IS (**Figure 6D**) or TSP1 (Supplemental Figure 5B), and the response was decreased by TSP1 siRNA or αTSP1Ab (**Figure 6E**). Morphometric analysis revealed significant increases in HCM surface area in response to TSP1 or IS, and effect of IS was again mitigated with TSP1 siRNA (**Figure 6F**). TSP1, but not IS, significantly increases the messenger level of atrial and brain natriuretic peptides in HCMs (**Figure 6G**).

IS down-regulated HCM metabolic activity (measured via MTT [3-(4,5-dimethylthiazol-2-yl)-2,5-diphenyl-2H-tetrazolium bromide] incorporation) at all concentrations (**Figure 7A**), and TSP1 demonstrated an effect at 2.2 nmol/L (**Figure 7B**). TSP1 siRNA treatment reduced IS-induced effects (**Figure 7C**). Limited synthetic capability reflects cellular senescence, and prematurely senescent cardiomyocytes accumulate in cardiomyopathies,[50] becoming pathogenic by introducing chronic inflammation (also known as SASP). HCM senescence in the context of uremic toxins has not been previously explored. IS (**Figure 7D**) and TSP1 (**Figure 7E**) significantly increased senescence-associated β-galactosidase in HCMs, and the effect was abrogated by siRNA (**Figure 7F**) or αTSP1Ab (**Figure 7G**). Messenger RNA levels of interleukin-6 and -1β, TNF-α, and CCL2 were increased following incubation with IS (**Figure 7H**) and decreased when cells were pretreated with αTSP1Ab.

We also investigated the effect of TSP1 on human cardiac fibroblasts, demonstrating a small, but significant decreased MTT incorporation (Supplemental Figure 6A) and increased senescence (Supplemental Figure 6B).

TSP1 AND AhR ARE RELEVANT IN HUMAN CRS. We have previously published that plasma TSP1 levels inversely correlate with estimated glomerular filtration rate.[19] Analysis of a subgroup of these patients (Supplemental Table 2) demonstrated an inverse relationship between plasma TSP1 and LVEF, as well as a direct correlation between plasma TSP1 and LV mass index (**Figure 8A**). There was no significant correlation between plasma TSP1 and fractional

FIGURE 6 **IS Induces Cardiomyocyte Hypertrophy That Is Dependent on TSP1**

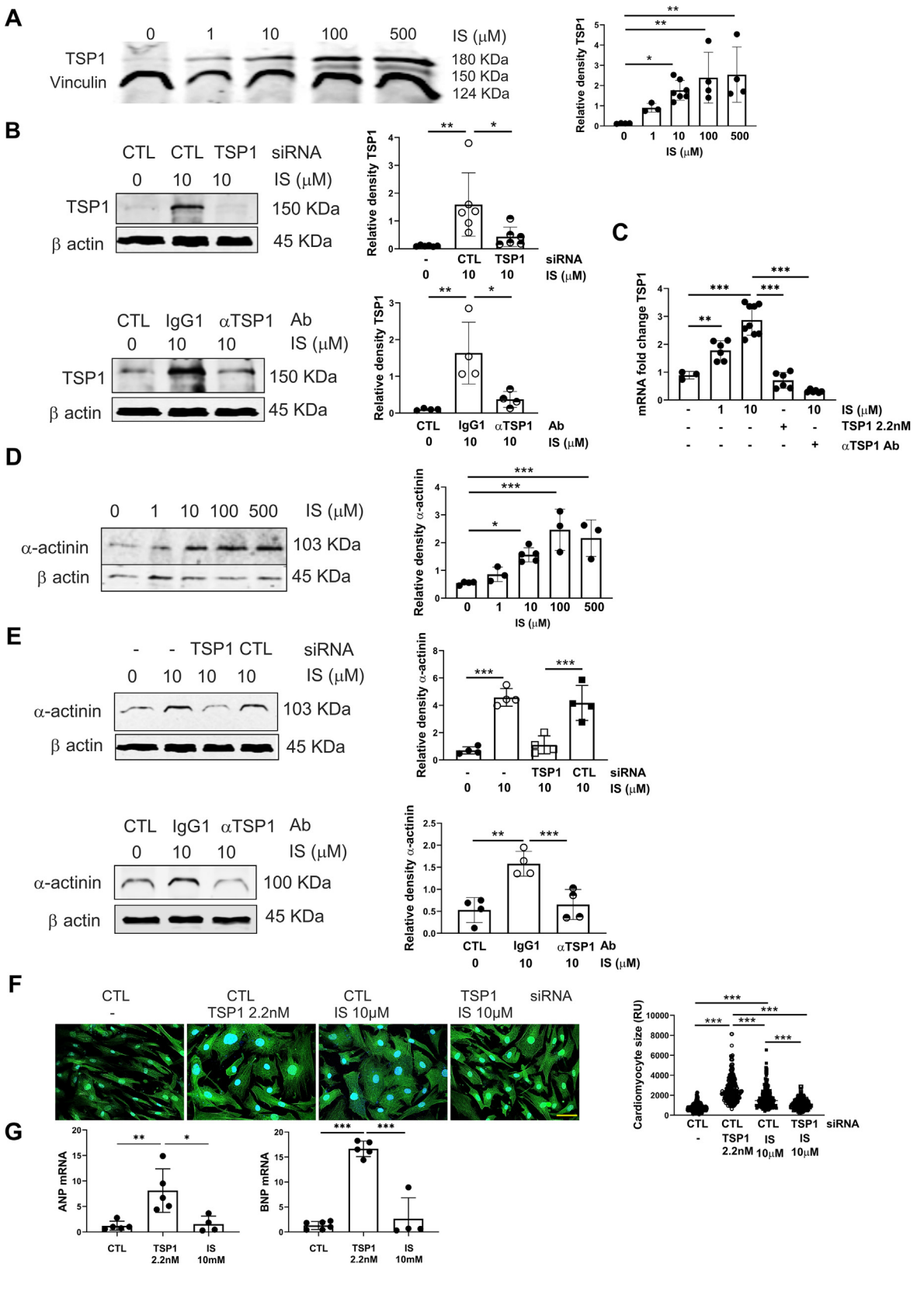

Continued on the next page

shortening, LV internal end-diastolic diameter, or end-systolic diameter (Supplemental Figure 7A).

The publicly available data set GSE160145 (Gene Expression Omnibus) provides gene expression data from explanted hearts from healthy or dialysis-dependent patients with CRS. The principal component analysis is shown in Supplemental Figure 7B. TSP1 and AhR gene expression was significantly up-regulated in patients with CKD compared to healthy control subjects (**Figure 8B**). DEGs between healthy and CRS hearts, including TSP1 and AhR, were identified in a volcano plot (**Figure 8C**). A heatmap from a subset of CRS patients also demonstrates the distribution of DEGs (Supplemental Figure 7C). The top 12 DEGs in CRS hearts are listed in Supplemental Table 3. A Wilcoxon rank-sum test was performed on candidate DEGs to establish enriched pathways in the Kyoto Encyclopedia of Genes and Genomes database (**Figure 8D**). DEGs were predominantly enriched in cytokine- and ECM-receptor interactions, as well as p53 signaling. Gene set enrichment analysis was also used to determine enriched pathways within the Gene Ontology database (Supplemental Figure 7D), demonstrating changes in cell cycle processes, oxidative stress, and senescence.

DISCUSSION

The excess burden of cardiac disease in renal impairment is well established, and patients experience morbidity and mortality from cardiovascular events rather than renal failure per se.[1] Uremia-specific toxins, particularly IS, are involved in the pathogenesis of CRS, and here we show, for the first time, that the matrix protein TSP1 is necessary to drive cardiac pathology. In vivo, WT mice subject to 5/6Nx demonstrated LVH, diastolic dysfunction, up-regulated myocardial TSP1 and AhR expression, maladaptive oxidative stress, SASP, and fibrosis. TSP1KO mice were protected from cardiac pathology despite equivalent renal dysfunction. Our in vitro results demonstrated that IS, through TSP1, promoted cardiomyocyte hypertrophy and SASP with activation of ERK and up-regulated AhR. Importantly, blockade of TSP1 signaling reversed abnormal cardiomyocyte findings associated with IS exposure. Analysis of an independent RNA-sequencing data set from explanted human hearts showed increased expression of TSP1 and AhR in samples with CRS patients (compared to healthy control subjects). Differential gene expression analysis in CRS hearts were linked with cytokine, extracellular matrix, and p53 signaling pathways, which we identified as relevant signaling pathways in vivo and in vitro. We believe these data uncover a novel mechanism that implicates TSP1 as a driver of LVH, positioning it as a potential biomarker of disease and a prospective target for clinical intervention.

Our findings are clinically relevant: we have previously published that plasma TSP1 correlated inversely with estimated glomerular filtration rate.[19] We extended these findings to demonstrate correlation with both reduced EF and increased LV mass. Large cohort studies have previously published that patients with CKD can present with HFpEF or HF with reduced EF, and similar relationships were observed for estimated glomerular filtration rate and proteinuria in terms of all-cause hospitalization regardless of EF.[51,52] There are also reports of bimodal presentations of EF in CKD patient populations with an increased prevalence of HFpEF.[52,53] Consistent with a recent report,[54] we observed diastolic dysfunction and markers of HFpEF only in WT-5/6Nx mice, which might be a function of animal age (<6 months old),

FIGURE 6 Continued

(A) Human cardiomyocytes were treated with IS at 0 μmol/L (n = 3), 1 μmol/L (n = 3), 10 μmol/L (n = 7), 100 μmol/L (n = 4), and 500 μmol/L (n = 4) for 24 hours. TSP1 and vinculin were measured by Western blotting in whole-cell lysates. Band density was normalized with vinculin. (B) Human cardiomyocytes were transfected with CTL or TSP1 siRNA (50 nmol/L), or treated with isotype control IgG_1 or αTSP1Ab antibody (1 μg/mL), incubated with IS (10 μmol/L), then probed for TSP1 protein or TSP1 mRNA expression (C). (D) Human cardiomyocytes were treated with increasing doses of IS and probed for α-actinin. (E) Human cardiomyocytes were transfected with CTL or αTSP1 siRNA (50 nmol/L) or treated with IgG_1 or αTSP1Ab (1 μg/mL), incubated with IS (10 μmol/L), then probed for α-actinin. Band density was normalized with β-actin. Representative Western blots and combined densitometry are shown (n = 3-7). (F) Human cardiomyocyte surface area after treatment with TSP1 (2.2 nmol/L) or IS (10 μmol/L) for 48 hours, following transfection with CTL or TSP1 siRNA (50 nmol/L) for 48 hours. Cells were stained for α-actinin (green) and 4′,6-diamidino-2-phenylindole (blue) (original magnification 40×; bar = 50 μm). Measurements are from 233 to 259 randomly chosen cells from 4 independent experiments. (G) Human cardiomyocytes were treated with TSP1 (2.2 nmol/L) and IS (10 μmol/L) for 24 hours and were probed for atrial natriuretic peptide (ANP) and brain natriuretic peptide (BNP) mRNA (n = 4-6). All data are mean ± SD; *$P < 0.05$, **$P < 0.01$, and ***$P < 0.001$ by 1-way analysis of variance with Sidak multiple comparisons test. RU = relative units; other abbreviations as in **Figures 1, 2, and 4**.

FIGURE 7 IS induces HCM SASP That Is Dependent on TSP1

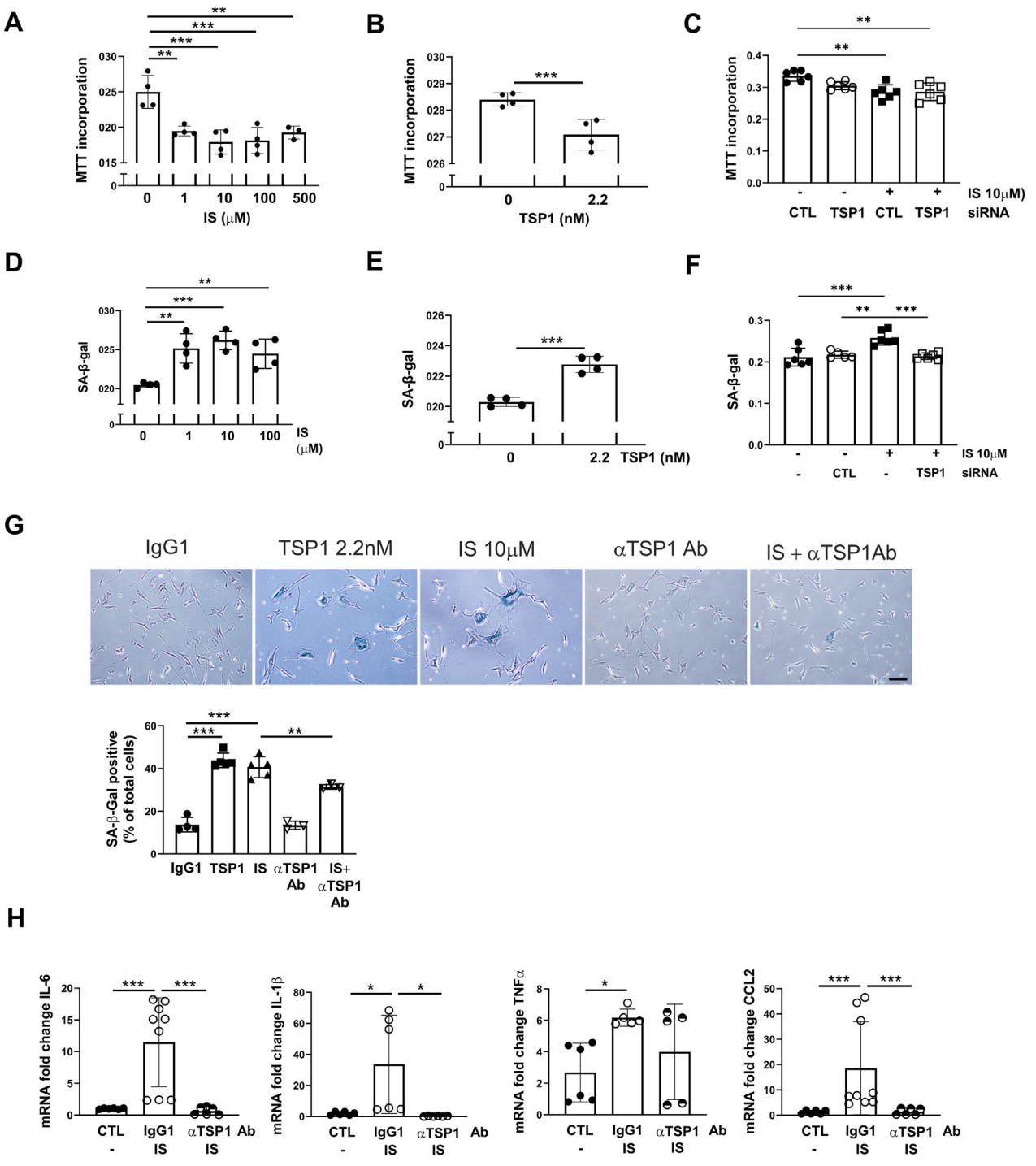

Incorporation of 3-(4,5-dimethylthiazol-2-yl)-2,5-diphenyl-2H-tetrazolium bromide (MTT) in human cardiomyocytes (HCMs) following incubation with (A) IS (1, 10, 100, and 500 μmol/L), (B) TSP1 (2.2 nmol/L), or (C) IS (10 μmol/L) following transfection with CTL or TSP1 siRNA (50 nmol/L) (n = 3-6). HCM senescence-associated β-galactosidase (SA-β-gal) activity following (D) IS (1, 10, and 100 μmol/L), (E) TSP1 (2.2 nmol/L), or (F) IS pretreated with CTL or TSP1 siRNA (50 nmol/L) (n = 5-6). (G) SA-β-gal staining following incubation with TSP1 (2.2 nmol/L) (n = 5), IS (10 μmol/L) (n = 5), IgG_1 antibody (1 μg/mL) (n = 4) or αTSP1Ab (1 μg/mL) (n = 3). Measurements are from 5 randomly chosen images from independent experiments (bar = 200 μm). (H) Transcript expression of IL-6, IL-1, TNF, and CCL2 from HCMs treated with IS, CTL antibody or αTSP1Ab (n = 3 independent experiments, normalized to 18S ribosome). All data are mean ± SD; *$P < 0.05$, **$P < 0.01$, and ***$P <$ 0.001 by 1-way analysis of variance with Sidak multiple comparisons test (A, C, D, F to H) or Student's *t*-test (B, E). SASP = senescence-associated secretory phenotype; other abbreviations as in Figures 1 to 4.

FIGURE 8 **TSP1 and AhR Expression Is Up-Regulated in Diseased Human Hearts**

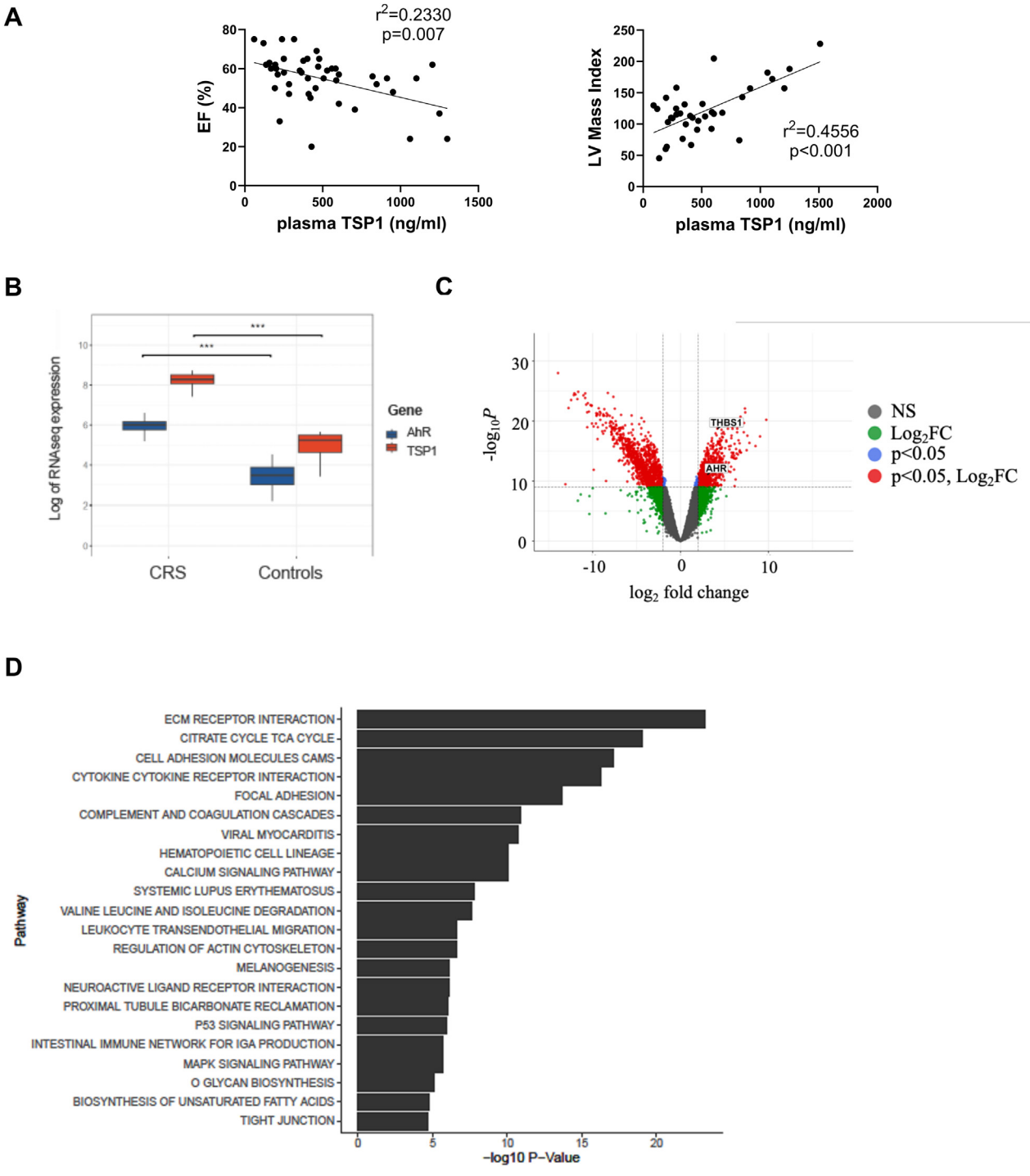

(A) Linear regression analysis of plasma TSP1 levels and percentage of EF or left ventricular (LV) mass index in patients with chronic kidney disease. (B) Range of TSP1 and AhR gene expression in explanted hearts from healthy patients compared to those with cardiorenal syndrome. Data are expressed as median with 25th and 75th percentiles (box plot); ***$P < 0.001$ by Wilcoxon rank-sum test. (C) Volcano plot of differentially expressed genes from RNA-sequencing (RNA-seq)-analyzed explanted hearts from healthy patients or those with cardiorenal syndrome. (D) Kyoto Encyclopedia of Genes and Genomes pathway of differentially expressed genes. CAMS = cell-cell adhesion molecules; ECM = extracellular matrix; FC = fold change; IGA = immunoglobulin A; NS = not significant; TCA = citric acid cycle; other abbreviations as in Figures 1 and 3 to 5.

genotype (C57BL/6 background), diet (standard chow), and duration of CKD (12 weeks). Other features, including impaired exercise capacity caused by skeletal muscle weakness, malnutrition (failure to gain weight), inflammation, and dehydration (due to polyuria),[55,56] may be additional confounding factors, and these require further investigation.

TSP1 is a matrix glycoprotein produced by numerous cell types[18,25,57] that activates transforming growth factor-β to induce fibrosis,[57] limits cellular proliferation,[49] increases redox stress,[25] and promotes inflammatory responses,[58] all of which we demonstrate in the cardiac pathology of our murine CRS model. In this study, we also establish that TSP1 is upstream of ERK1/2 activation and AhR (with likely bidirectional signaling), which are complicit in the development of SASP and cardiac dysfunction. Our use of a global TSP1KO mouse did not define the cell type responsible for TSP1 secretion, although we focused on cardiomyocyte phenotype in vitro. However, all nucleated cells produce TSP1 in response to external stressors[59] (eg, hypoxia, inflammation, hyperglycemia), and it may be that paracrine signaling, particularly SASP-derived products,[10] among cardiomyocytes, fibroblasts, and endothelial cells, cooperatively contributes to adverse cardiac remodeling.[60]

We were able to definitively demonstrate a permissive cardiorenal phenotype following 5/6Nx in WT mice. The 5/6Nx model is typically associated with high mortality,[20] presumably due to acute uremia following excision of the contralateral kidney. However, alterations in our surgical technique significantly improved survival to >85%-90%. TSP1KO mice are resistant to acute kidney injury;[61] therefore, the induction of equivalent renal injury through a reduction in functional renal parenchyma was only possible using a 5/6Nx model. Measurements of renal dysfunction were equivalent, supporting the use of global KO animals for this study.

Accumulated toxins are the cause of uremia in CKD, and robust evidence establishes uremic toxins as central to the deranged molecular pathways in both CVD and CKD.[14] IS is the best characterized uremic toxin, from both epidemiologic and molecular perspectives. It promotes expression of profibrotic genes (through Smad-dependent transforming growth factor-β),[57,62] up-regulating inflammation[63] and cellular senescence[64,65] via reactive oxygen species and p53 pathways[66,67] (although not demonstrated in cardiomyocytes). Interestingly, the cellular effects of IS mimic those seen with TSP1, but the role of TSP1 in CKD-induced cardiac pathology is unexplored. In this study, absence of TSP1 attenuated features of CRS-induced LVH and mitigated expression of deranged molecular pathways without altering blood pressure, supporting a cardiac effect that is independent of the vasculature (but not necessarily vascular responsiveness).

We have previously reported the induction of cardiac TSP1 in animal models with right ventricular dysfunction,[18] and disruption of TSP1 signaling provided cardioprotection in the same setting.[68] However, the role of TSP1 in preclinical models of pressure overload–induced LV dysfunction is discordant,[69,70] with TSP1KO mice exhibiting early hypertrophy and late dilation despite less type 1 collagen deposition.[69,70] However, our CRS model is not defined by increased afterload (hypertension), which is consistent with published reports.[21,71,72] Histopathologic studies have shown that cardiomyocyte diameter and resting tension are both increased in HFpEF.[73-75] Higher cardiomyocyte resting tension has been presumably related to sarcomeric protein phosphorylation that was observed in patients[75] and preclinical models.[76] In our study, both myocyte diameter and sarcomeric actinin were increased in WT-5/6Nx mice, but were mitigated in TSP1KO-5/6Nx mice. Diastolic dysfunction can result from abnormal relaxation and/or increased myocardial stiffness, ultimately leading to elevated LV filling pressures and HFpEF. LV filling pressure is assessed by E/A, isovolumetric relaxation time, and the E/e′ ratio, which constitutes key hemodynamic abnormalities associated with diastolic dysfunction. These parameters can effectively stratify HF phenotypes, including those with both reduced and preserved EF,[77-79] and have been applied in small animal studies.[80] In our study, E/A, isovolumetric relaxation time, and E/e′ ratio were increased in WT-5/6Nx mice but not in TSP1KO-5/6Nx mice.

STUDY LIMITATIONS. Uremia is a complex condition with multiple systemic abnormalities, including cardiomyopathy. Animal models, including 5/6Nx may not fully mimic the progressive nature of human uremic cardiomyopathy owing to differences in comorbid conditions, including hypertension. Differences in disease duration and severity of kidney injury can also affect the relevance of research findings.

The tissue architecture and mechanical cues in the heart and blood vessels influence cellular phenotype and cross-talk, but these factors are absent in cell culture systems, limiting the relevance of findings. Uremic cardiomyopathy involves interactions among multiple cell types, which may not be fully captured when studying cell types individually. Further

studies are required to accurately define the culprit cell promoting the cardiac pathology seen in CRS. In addition, lack of concurrent clinical details in the patient cohort warrant large clinical studies that will appropriately define the place of TSP1 as a potential biomarker of disease.

CONCLUSIONS

Collectively our results suggest that TSP1 is driving the cellular effects of IS through activation of ERK and AhR, supporting our hypothesis that TSP1 is a missing link between CKD and development of CVD, particularly LVH. The mechanisms that underscore its development include oxidative stress, senescence, and inflammation.

ACKNOWLEDGMENTS The authors are grateful to Pre-Clinical Imaging Facility, Sydney Imaging Core Research Facility (Charles Perkins Centre, The University of Sydney) for small animal imaging. The authors appreciate the facilities, resources, and professional assistance provided by the Westmead Institute for Medical Research Histology and Cell Imaging Facilities. The authors thank Drs Jennifer Li and Kedar Ghimire (Westmead Institute for Medical Research) for valuable assistance with the manuscript.

FUNDING SUPPORT AND AUTHOR DISCLOSURES

This work was supported by a National Health Medical Research Council grant (GNT2007991) to awarded to Dr Rogers, a National Heart Foundation Vanguard Grant (106035) to Drs Rogers and Julovi, and a Westmead Medical Research Foundation grant to Dr Julovi. All other authors have reported that they have no relationships relevant to the contents of this paper to disclose.

ADDRESS FOR CORRESPONDENCE: Prof Natasha M. Rogers, Kidney Injury Group, Centre for Transplant and Renal Research, Westmead Institute for Medical Research, 176 Hawkesbury Road, Westmead, New South Wales 2145, Australia. E-mail: natasha.rogers@health.nsw.gov.au. OR Dr Sohel M. Julovi, Kidney Injury Group, Centre for Transplant and Renal Research, Westmead Institute for Medical Research, 176 Hawkesbury Road, Westmead, New South Wales 2145, Australia. E-mail: sohel.julovi@sydney.edu.au.

PERSPECTIVES

COMPETENCY IN MEDICAL KNOWLEDGE: Patients with CKD continue to experience dramatically reduced life expectancy owing to concomitant CVD, termed CRS. Despite a consensus definition, there has been minimal progress in our understanding of the pathophysiology and no specific therapeutic interventions that improve outcomes. Here we demonstrate that the uremic toxin IS is driving deleterious changes in cardiomyocyte phenotype through the matrix protein TSP1. These findings provide a potential therapeutic target for CRS.

TRANSLATIONAL OUTLOOK: Patients with HFpEF are vulnerable to the development of renal dysfunction during treatment for decompensation, and renal-associated mortality is higher in patients with HFpEF. We have identified a novel pathway that drives uremic toxin-induced changes in cardiac pathology through the protein TSP1. Our mechanistic data lend support for testing monoclonal antibodies or peptidic inhibitors that block the actions of TSP1 (and therefore IS), limit development of LVH, and potentially improve survival in CRS.

REFERENCES

1. Jha V, Garcia-Garcia G, Iseki K, et al. Chronic kidney disease: global dimension and perspectives. *Lancet*. 2013;382(9888):260–272.

2. Vanholder R, Massy Z, Argiles A, et al. Chronic kidney disease as cause of cardiovascular morbidity and mortality. *Nephrol Dial Transplant*. 2005;20(6):1048–1056.

3. Rangaswami J, Bhalla V, Blair JEA, et al. Cardiorenal syndrome: classification, pathophysiology, diagnosis, and treatment strategies: a scientific statement from the American Heart Association. *Circulation*. 2019;139(16):e840–e878.

4. Taveira Gomes T, Santos Araujo C, Valente F, et al. Cardiorenal syndrome and death risk in patients with heart failure or chronic kidney disease: an unmet cardiorenal need? *Eur Heart J*. 2021;42(suppl 1):819.

5. Deo R, Fyr CL, Fried LF, et al, Health ABC study. Kidney dysfunction and fatal cardiovascular disease—an association independent of atherosclerotic events: results from the Health, Aging, and Body Composition (Health ABC) study. *Am Heart J*. 2008;155(1):62–68.

6. Unger ED, Dubin RF, Deo R, et al. Association of chronic kidney disease with abnormal cardiac mechanics and adverse outcomes in patients with heart failure and preserved ejection fraction. *Eur J Heart Fail*. 2016;18(1):103–112.

7. Hillege HL, Nitsch D, Pfeffer MA, et al. CHARM Investigators. Renal function as a predictor of outcome in a broad spectrum of patients with heart failure. *Circulation*. 2006;113(5):671–678.

8. Gallo S, Vitacolonna A, Bonzano A, Comoglio P, Crepaldi T. ERK: a key player in the pathophysiology of cardiac hypertrophy. *Int J Mol Sci*. 2019;20(9):2164.

9. Anderson G, Mazzoccoli G. Left ventricular hypertrophy: roles of mitochondria CYP1B1 and melatonergic pathways in co-ordinating wider pathophysiology. *Int J Mol Sci*. 2019;20(16):4068.

10. Mehdizadeh M, Aguilar M, Thorin E, Ferbeyre G, Nattel S. The role of cellular senescence in cardiac disease: basic biology and clinical relevance. *Nat Rev Cardiol*. 2022;19(4):250–264.

11. Tumur Z, Niwa T. Indoxyl sulfate inhibits nitric oxide production and cell viability by inducing oxidative stress in vascular endothelial cells. *Am J Nephrol*. 2009;29(6):551–557.

12. Barreto FC, Barreto DV, Liabeuf S, et al, EUTox Work Group. Serum indoxyl sulfate is associated with vascular disease and mortality in chronic kidney disease patients. *Clin J Am Soc Nephrol*. 2009;4(10):1551–1558.

13. Lekawanvijit S. Cardiotoxicity of uremic toxins: a driver of cardiorenal syndrome. *Toxins (Basel)*. 2018;10(9):352.

14. Hung SC, Kuo KL, Wu CC, Tarng DC. Indoxyl sulfate: a novel cardiovascular risk factor in chronic kidney disease. *J Am Heart Assoc*. 2017;6(2):e005022.

15. Parfrey PS, Harnett JD, Foley RN, et al. Impact of renal transplantation on uremic cardiomyopathy. *Transplantation*. 1995;60(9):908–914.

16. Rogers NM, Sharifi-Sanjani M, Csanyi G, Pagano PJ, Isenberg JS. Thrombospondin-1 and CD47 regulation of cardiac, pulmonary and vascular responses in health and disease. *Matrix Biol*. 2014;37:92–101.

17. Frangogiannis NG. The extracellular matrix in ischemic and nonischemic heart failure. *Circ Res*. 2019;125(1):117–146.

18. Rogers NM, Sharifi-Sanjani M, Yao M, et al. TSP1-CD47 signaling is upregulated in clinical pulmonary hypertension and contributes to pulmonary arterial vasculopathy and dysfunction. *Cardiovasc Res*. 2017;113(1):15–29.

19. Julovi S, Sanganeria B, Minhas N, Ghimire K, Nankivell B, Rogers NM. Blocking thrombospondin-1 signaling via CD47 mitigates renal interstitial fibrosis. *Lab Invest*. 2020;100(9):1184–1196.

20. Rosendahl A, Kabiri R, Bode M, et al. Adaptive immunity and IL-17A are not involved in the progression of chronic kidney disease after 5/6 nephrectomy in mice. *Br J Pharmacol*. 2019;176(12):2002–2014.

21. Julovi SM, Dao A, Trinh K, et al. Disease-modifying interactions between chronic kidney disease and osteoarthritis: a new comorbid mouse model. *RMD Open*. 2023;9(3):e003109.

22. Zacchigna S, Paldino A, Falcão-Pires I, et al. Towards standardization of echocardiography for the evaluation of left ventricular function in adult rodents: a position paper of the ESC Working Group on Myocardial Function. *Cardiovasc Res*. 2021;117(1):43–59.

23. Julovi SM, Martin JL, Baxter RC. Nuclear insulin-like growth factor binding protein-3 as a biomarker in triple-negative breast cancer xenograft tumors: effect of targeted therapy and comparison with chemotherapy. *Front Endocrinol (Lausanne)*. 2018;9:120.

24. Meijles DN, Sahoo S, Al Ghouleh I, et al. The matricellular protein TSP1 promotes human and mouse endothelial cell senescence through CD47 and Nox1. *Sci Signal*. 2017;10(501):eaaj1784.

25. Yao M, Rogers NM, Csanyi G, et al. Thrombospondin-1 activation of signal-regulatory protein-alpha stimulates reactive oxygen species production and promotes renal ischemia reperfusion injury. *J Am Soc Nephrol*. 2014;25(6):1171–1186.

26. Love MI, Huber W, Anders S. Moderated estimation of fold change and dispersion for RNA-seq data with DESeq2. *Genome Biol*. 2014;15(12):550.

27. KEGG pathway database: wiring diagrams of molecular interactions, reactions and relations. Kyoto Encyclopedia of Genes and Genomes. Accessed February 15, 2021. https://www.genome.jp/kegg/pathway.html

28. Yu G, Wang LG, Han Y, He QY. clusterProfiler: an R package for comparing biological themes among gene clusters. *OMICS*. 2012;16(5):284–287.

29. The Gene Ontology Resource. Gene Ontology. Accessed February 15, 2021. http://geneontology.org

30. Robertson H. Thrombospondin-1-drives-cardiac-remodelling-in-chronic-kidney-disease. Accessed February 15, 2021. https://github.com/Harry25R/Thrombospondin-1-drives-cardiac-remodelling-in-chronic-kidney-disease

31. Kennedy DJ, Vetteth S, Periyasamy SM, et al. Central role for the cardiotonic steroid marinobufagenin in the pathogenesis of experimental uremic cardiomyopathy. *Hypertension*. 2006;47(3):488–495.

32. Izumo S, Lompre AM, Matsuoka R, et al. Myosin heavy chain messenger RNA and protein isoform transitions during cardiac hypertrophy. Interaction between hemodynamic and thyroid hormone-induced signals. *J Clin Invest*. 1987;79(3):970–977.

33. van Bilsen M, Chien KR. Growth and hypertrophy of the heart: towards an understanding of cardiac specific and inducible gene expression. *Cardiovasc Res*. 1993;27(7):1140–1149.

34. Kostin S, Hein S, Arnon E, Scholz D, Schaper J. The cytoskeleton and related proteins in the human failing heart. *Heart Fail Rev*. 2000;5(3):271–280.

35. Takimoto E, Kass DA. Role of oxidative stress in cardiac hypertrophy and remodeling. *Hypertension*. 2007;49(2):241–248.

36. Yokoyama T, Nakano M, Bednarczyk JL, McIntyre BW, Entman M, Mann DL. Tumor necrosis factor-alpha provokes a hypertrophic growth response in adult cardiac myocytes. *Circulation*. 1997;95(5):1247–1252.

37. Damera S, Raphael KL, Baird BC, Cheung AK, Greene T, Beddhu S. Serum alkaline phosphatase levels associate with elevated serum C-reactive protein in chronic kidney disease. *Kidney Int*. 2011;79(2):228–233.

38. Kunutsor SK, Apekey TA, Khan H. Liver enzymes and risk of cardiovascular disease in the general population: a meta-analysis of prospective cohort studies. *Atherosclerosis*. 2014;236(1):7–17.

39. Sabri A, Hughie HH, Lucchesi PA. Regulation of hypertrophic and apoptotic signaling pathways by reactive oxygen species in cardiac myocytes. *Antioxid Redox Signal*. 2003;5(6):731–740.

40. Muslin AJ. MAPK signalling in cardiovascular health and disease: molecular mechanisms and therapeutic targets. *Clin Sci (Lond)*. 2008;115(7):203–218.

41. Chen Y, Leask A, Abraham DJ, et al. Thrombospondin 1 is a key mediator of transforming growth factor beta-mediated cell contractility in systemic sclerosis via a mitogen-activated protein kinase kinase (MEK)/extracellular signal-regulated kinase (ERK)-dependent mechanism. *Fibrogenesis Tissue Repair*. 2011;4(1):9.

42. Suchard SJ, Burton MJ, Dixit VM, Boxer LA. Human neutrophil adherence to thrombospondin occurs through a CD11/CD18-independent mechanism. *J Immunol*. 1991;146(11):3945–3952.

43. Annis DS, Murphy-Ullrich JE, Mosher DF. Function-blocking antithrombospondin-1 monoclonal antibodies. *J Thromb Haemost*. 2006;4(2):459–468.

44. Dou L, Poitevin S, Sallee M, et al. Aryl hydrocarbon receptor is activated in patients and mice with chronic kidney disease. *Kidney Int*. 2018;93(4):986–999.

45. Kim JB, Pjanic M, Nguyen T, et al. TCF21 and the environmental sensor aryl-hydrocarbon receptor cooperate to activate a pro-inflammatory gene expression program in coronary artery smooth muscle cells. *PLoS Genet*. 2017;13(5):e1006750.

46. Dabir P, Marinic TE, Krukovets I, Stenina OI. Aryl hydrocarbon receptor is activated by glucose and regulates the thrombospondin-1 gene promoter in endothelial cells. *Circ Res*. 2008;102(12):1558–1565.

47. Tan Z, Chang X, Puga A, Xia Y. Activation of mitogen-activated protein kinases (MAPKs) by aromatic hydrocarbons: role in the regulation of aryl hydrocarbon receptor (AHR) function. *Biochem Pharmacol*. 2002;64(5-6):771–780.

48. Vanholder R, De Smet R, Glorieux G, et al, EUTox Work Group. Review on uremic toxins: classification, concentration, and interindividual variability. *Kidney Int*. 2003;63(5):1934–1943.

49. Rogers NM, Zhang ZJ, Wang JJ, Thomson AW, Isenberg JS. CD47 regulates renal tubular epithelial cell self-renewal and proliferation following renal ischemia reperfusion. *Kidney Int*. 2016;90(2):334–347.

50. Predmore JM, Wang P, Davis F, et al. Ubiquitin proteasome dysfunction in human hypertrophic and dilated cardiomyopathies. *Circulation*. 2010;121(8):997–1004.

51. Smith DH, Thorp ML, Gurwitz JH, et al. Chronic kidney disease and outcomes in heart failure with preserved versus reduced ejection fraction: the Cardiovascular Research Network PRESERVE Study. *Circ Cardiovasc Qual Outcomes*. 2013;6(3):333–342.

52. Owan TE, Hodge DO, Herges RM, Jacobsen SJ, Roger VL, Redfield MM. Trends in prevalence and outcome of heart failure with preserved ejection fraction. *N Engl J Med*. 2006;355(3):251–259.

53. Borlaug BA, Redfield MM. Diastolic and systolic heart failure are distinct phenotypes within the heart failure spectrum. *Circulation*. 2011;123(18):2006–2013 [discussion: 2014].

54. Sárközy M, Watzinger S, Kovács Z, et al. Neuregulin-1β improves uremic cardiomyopathy and renal dysfunction in rats. *J Am Coll Cardiol Basic Trans Science*. 2023;8(9):1160–1176. https://doi.org/10.1016/j.jacbts.2023.03.003

55. Himmelfarb J, Stenvinkel P, Ikizler TA, Hakim RM. The elephant in uremia: oxidant stress as a unifying concept of cardiovascular disease in uremia. *Kidney Int*. 2002;62(5):1524–1538.

56. Stohr EJ, Gonzalez-Alonso J, Pearson J, et al. Dehydration reduces left ventricular filling at rest and during exercise independent of twist mechanics. *J Appl Physiol (1985)*. 2011;111(3):891–897.

57. Murphy-Ullrich JE, Poczatek M. Activation of latent TGF-beta by thrombospondin-1: mechanisms and physiology. *Cytokine Growth Factor Rev*. 2000;11(1-2):59–69.

58. Frangogiannis NG, Ren G, Dewald O, et al. Critical role of endogenous thrombospondin-1 in preventing expansion of healing myocardial infarcts. *Circulation*. 2005;111(22):2935–2942.

59. Stenina-Adognravi O. Invoking the power of thrombospondins: regulation of thrombospondins expression. *Matrix Biol*. 2014;37:69–82.

60. Tang X, Li PH, Chen HZ. Cardiomyocyte senescence and cellular communications within myocardial microenvironments. *Front Endocrinol (Lausanne)*. 2020;11:280.

61. Thakar CV, Zahedi K, Revelo MP, et al. Identification of thrombospondin 1 (TSP-1) as a novel mediator of cell injury in kidney ischemia. *J Clin Invest*. 2005;115(12):3451–3459.

62. Lekawanvijit S, Adrahtas A, Kelly DJ, Kompa AR, Wang BH, Krum H. Does indoxyl sulfate, a uraemic toxin, have direct effects on cardiac fibroblasts and myocytes? *Eur Heart J*. 2010;31(14):1771–1779.

63. Sun CY, Hsu HH, Wu MS. p-Cresol sulfate and indoxyl sulfate induce similar cellular inflammatory gene expressions in cultured proximal renal tubular cells. *Nephrol Dial Transplant*. 2013;28(1):70–78.

64. Adijiang A, Higuchi Y, Nishijima F, Shimizu H, Niwa T. Indoxyl sulfate, a uremic toxin, promotes cell senescence in aorta of hypertensive rats. *Biochem Biophys Res Commun*. 2010;399(4):637–641.

65. Shimizu H, Yisireyili M, Nishijima F, Niwa T. Indoxyl sulfate enhances p53-TGF-beta1-Smad3 pathway in proximal tubular cells. *Am J Nephrol*. 2013;37(2):97–103.

66. Adelibieke Y, Shimizu H, Saito S, Mironova R, Niwa T. Indoxyl sulfate counteracts endothelial effects of erythropoietin through suppression of Akt phosphorylation. *Circ J*. 2013;77(5):1326–1336.

67. Shimizu H, Yisireyili M, Higashiyama Y, Nishijima F, Niwa T. Indoxyl sulfate upregulates renal expression of ICAM-1 via production of ROS and activation of NF-kappaB and p53 in proximal tubular cells. *Life Sci*. 2013;92(2):143–148.

68. Ochoa CD, Yu L, Al-Ansari E, Hales CA, Quinn DA. Thrombospondin-1 null mice are resistant to hypoxia-induced pulmonary hypertension. *J Cardiothorac Surg*. 2010;5:32.

69. Xia Y, Dobaczewski M, Gonzalez-Quesada C, et al. Endogenous thrombospondin 1 protects the pressure-overloaded myocardium by modulating fibroblast phenotype and matrix metabolism. *Hypertension*. 2011;58(5):902–911.

70. Belmadani S, Bernal J, Wei CC, et al. A thrombospondin-1 antagonist of transforming growth factor-beta activation blocks cardiomyopathy in rats with diabetes and elevated angiotensin II. *Am J Pathol*. 2007;171(3):777–789.

71. Bongartz LG, Braam B, Gaillard CA, et al. Target organ cross talk in cardiorenal syndrome: animal models. *Am J Physiol Renal Physiol*. 2012;303(9):F1253–F1263.

72. Nakano T, Katsuki S, Chen M, et al. Uremic toxin indoxyl sulfate promotes proinflammatory macrophage activation via the interplay of OATP2B1 and Dll4-Notch signaling. *Circulation*. 2019;139(1):78–96.

73. van Heerebeek L, Borbely A, Niessen HW, et al. Myocardial structure and function differ in systolic and diastolic heart failure. *Circulation*. 2006;113(16):1966–1973.

74. Borbely A, van der Velden J, Papp Z, et al. Cardiomyocyte stiffness in diastolic heart failure. *Circulation*. 2005;111(6):774–781.

75. van Heerebeek L, Hamdani N, Handoko ML, et al. Diastolic stiffness of the failing diabetic heart: importance of fibrosis, advanced glycation end products, and myocyte resting tension. *Circulation*. 2008;117(1):43–51.

76. Sheng JJ, Feng HZ, Pinto JR, Wei H, Jin JP. Increases of desmin and alpha-actinin in mouse cardiac myofibrils as a response to diastolic dysfunction. *J Mol Cell Cardiol*. 2016;99:218–229.

77. Paulus WJ, Tschope C, Sanderson JE, et al. How to diagnose diastolic heart failure: a consensus statement on the diagnosis of heart failure with normal left ventricular ejection fraction by the Heart Failure and Echocardiography Associations of the European Society of Cardiology. *Eur Heart J*. 2007;28(20):2539–2550.

78. Guazzi M, Dixon D, Labate V, et al. RV contractile function and its coupling to pulmonary circulation in heart failure with preserved ejection fraction: stratification of clinical phenotypes and outcomes. *J Am Coll Cardiol Img*. 2017;10(10 Pt B):1211–1221.

79. Mohammed SF, Hussain I, AbouEzzeddine OF, et al. Right ventricular function in heart failure with preserved ejection fraction: a community-based study. *Circulation*. 2014;130(25):2310–2320.

80. Hamdani N, Franssen C, Lourenco A, et al. Myocardial titin hypophosphorylation importantly contributes to heart failure with preserved ejection fraction in a rat metabolic risk model. *Circ Heart Fail*. 2013;6(6):1239–1249.

KEY WORDS aryl hydrocarbon receptor, cardiac fibrosis, chronic kidney disease, left ventricular hypertrophy, thrombospondin 1

APPENDIX For supplemental figures and tables, please see the online version of this paper.